공학박사 학위논문

Therapeutic Ceria Nanoparticles for Alzheimer's and Parkinson's Disease

알츠하이머와 파킨슨 질병에 치료 효과를 보이는
세리아 나노 입자

2018년 8월

서울대학교 대학원
화학생물공학부
권 혁 진

Therapeutic Ceria Nanoparticles for Alzheimer's and Parkinson's Disease

지도교수 현 택 환

이 논문을 공학박사학위논문으로 제출함

2018 년 5월

서울대학교 대학원
화학생물공학부
권 혁 진

권혁진의 박사학위논문을 인준함

2018 년 8월

위 원 장 장 정 식 (인)
부 위 원 장 현 택 환 (인)
위 원 김 병 수 (인)
위 원 한 지 숙 (인)
위 원 나 현 빈 (인)

Abstract

Therapeutic Ceria Nanoparticles for Alzheimer's and Parkinson's Disease

Hyek Jin Kwon

School of Chemical and Biological Engineering

The Graduate School

Seoul National University

Ceria nanoparticles with a size less than 5 nm have been identified as an effective antioxidant that can scavenge reactive oxygen species (ROS) and reactive nitrogen species (RNS) by redox cycles between Ce^{3+} (reduced) and Ce^{4+} (oxidized) states on their surface. Moreover, the catalytic activities of ceria nanoparticles are regenerative. For these reasons, they are very attractive for the development of potential therapeutics for various diseases induced by ROS-mediated oxidative stress. In chapter 1, ceria nanoparticle in medical application is introduced.

Chapter 2 describes mitochondria-targeting ceria nanoparticles as antioxidants for Alzheimer's disease. Mitochondrial oxidative stress is a key pathologic factor in neurodegenerative diseases, including Alzheimer's disease. Abnormal generation of ROS, resulting from mitochondrial dysfunction, can lead to neuronal cell death. Ceria (CeO_2) nanoparticles are known to function as strong and recyclable ROS scavengers by shuttling between Ce^{3+} and Ce^{4+} oxidation states. Consequently, targeting ceria nanoparticles selectively to mitochondria might be a promising therapeutic approach for neurodegenerative diseases. Here, I report the design and synthesis of Triphenylphosph-onium (TPP)-conjugated ceria nanoparticles that localize to

mitochondria and suppress neuronal death in a 5XFAD transgenic Alzheimer's disease mouse model. The TPP-conjugated ceria nanoparticles mitigate reactive gliosis and morphological mitochondria damage observed in these mice. Altogether, our data indicate that the TPP-conjugated ceria nanoparticles are a potential therapeutic candidate for mitochondrial oxidative stress in Alzheimer's disease.

In chapter 3, I describe ceria nanoparticle systems for selective scavenging of mitochondrial, intracellular, and extracellular reactive oxygen species in Parkinson's disease. Oxidative stress induced by ROS is one of the critical factors that involve in the pathogenesis and progression of many diseases. However, lack of proper techniques to scavenge ROS depending on their cellular localization limits a thorough understanding of the pathological effects of ROS. Here, I demonstrate the selective scavenging of mitochondrial, intracellular, and extracellular ROS using three different types of ceria nanoparticles (NPs), and its application to treat Parkinson's disease (PD). Our data show that scavenging intracellular or mitochondrial ROS inhibits the microglial activation and lipid peroxidation, while protecting the tyrosine hydroxylase (TH) in the striata of PD model mice. These results indicate the essential roles of intracellular and mitochondrial ROS in the

progression of PD. I anticipate that our ceria NP systems will serve as a useful tool for elucidating the functions of various ROS in diseases

Keywords: nanoparticle, biomedical application, ceria nanoparticle, Alzheimer's disease, mitochondria, Parkinson's disease, reactive oxygen species, reactive oxygen species scavenger, mitochondrial ROS, intracellular ROS, extracellular ROS,

Student number: 2013-30276

Contents

List of Schemes

List of Figures

Chapter 1. Introduction: Ceria Nanoparticles in Medical Applications

1.1 Introduction

Excessive production of ROS and RNS results in the increased oxidative stress, which plays a key role in the pathogenesis of many serious diseases, including ischemic stroke, retinal degenerative diseases, sepsis, cancers, vascular diseases, as well as neurodegenerative diseases.[1] Ceria nanoparticles with a size less than 5 nm have been identified as an effective antioxidant that can scavenge ROS and RNS by redox cycles between Ce^{3+} (reduced) and Ce^{4+} (oxidized) states on their surface. This Ce^{3+} and Ce^{4+} redox switching, like the redox metal ion mechanism in metalloenzymes, enables the ceria nanoparticles to react in ways similar to two essential antioxidant enzymes: superoxide dismutase and catalase.[2-4] This reactivity successfully applied to protect cells in vitro against superoxide (O^{2-}) and hydrogen peroxide (H_2O_2), which are two predominant forms of ROS, via the superoxide dismutase- and catalase-mimetic activities of ceria nanoparticles, respectively. Furthermore, the catalytic activities of ceria nanoparticles are regenerative. [2-4] For these reasons, they are very attractive for the development of potential

therapeutics for various diseases induced by ROS-mediated oxidative stress.[3,5,6]

1.2 Ceria nanoparticles for neurodegenerative disease therapy

One of the major applications of ceria nanoparticles is the treatment of neurodegenerative diseases. For example, Alzheimer's disease and Parkinson's disease are manifested by progressive neuronal cell loss, abnormal protein aggregation in the brain, and mitochondrial oxidative stress.[7,8] Oxidative stress is known to be responsible for the mitochondrial dysfunction and the neuronal cell death, which consequently lead to the pathogenesis of these diseases. Therefore, reducing the oxidative stress using the regenerative ROS-scavenging activities of ceria nanoparticles can provide a unique treatment opportunity. Recent studies successfully demonstrated the use of ceria nanoparticles to protect neuron cells against superoxide and hydrogen peroxide in vitro and in vivo. For example, ceria nanoparticles targeting mitochondrial ROS were reported as a potential therapeutic for AD.[9] In this study, Triphenylphosphonium (TPP) was conjugated onto the ceria nanoparticles to allow the localization of the nanoparticles in

mitochondria. The TPP-conjugated ceria nanoparticles were injected into the subicula of transgenic AD mice (5XFAD). After two months, much less mitochondrial damage and neuronal cell death were observed in the mice treated with the TPP-conjugated ceria nanoparticles compared with the sham group, indicating that the TPP-conjugated ceria nanoparticles could protect mitochondria from oxidative stress by scavenging mitochondrial ROS. Although these findings are promising, the inability of most nanoparticles to cross the blood–brain barrier (BBB) due to their relatively larger size than small molecules remain an obstacle for noninvasive treatment of neurodegenerative diseases.

1.3 Ceria nanoparticles for Ischemic stroke therapy

Ischemic stroke is caused by a blockage or serious reduction of blood supply to the brain, accompanied by the dysfunction of brain tissues.[10] A cascade of events that increase ROS production occur during the process. Moreover, a considerable amount of hydrogen peroxide and other reactive species such as hydroperoxyl radicals are converted from superoxide anions in acidic condition owing to the accumulation of lactic acid from energy depletion.[10] Therefore, reducing cerebral oxidative stress by decreasing the excessively produced ROS can be an effective

strategy for the ischemic stroke therapy. In a recent study, ceria nanoparticles coated with phospholipid-PEG (PLPEG-ceria) were shown to protect neuron cells from ischemic stroke injury in an in vivo rat model.[11] The PLPEG-ceria nanoparticles showed good colloidal stability with reduced nonspecific binding and maintained their regenerative ROS-scavenging activities in blood plasma. This study induced brain ischemia through extensive breakage of BBB, which allowed the intravenously injected PLPEG-ceria nanoparticles to reach the brain. After the permeation of the nanoparticles into the brain tissues, the infarct volume, oxidative stress, and population of apoptotic cells were significantly decreased compared with those of the control group.

1.4 Ceria nanoparticles for retinal degenerative disease therapy

Ceria nanoparticles have also been used to treat retinal degenerative diseases.[12] Since the retina consumes a very large amount of oxygen, its microenvironment contains relatively high levels of oxygen, which can be a source of ROS generation. Moreover, the presence of abundant photosensitizers, light exposure, and the high energy demand all promote a highly oxidative microenvironment in the retina, producing ROS that

can be detrimental to the photoreceptor cells. Therefore, protecting photoreceptor cells from the oxidative stress in the retina is critical for the prevention and treatment of retinal degenerative diseases, including inherited retinal degeneration, diabetic retinopathy, macular degeneration, and retinal detachment.[12] Chen et al. investigated the protective effect of ceria nanoparticles on retinal functions and photoreceptor cells against light-induced damages using an albino rat model, where ceria nanoparticles were injected intravitreally.[13] Retinal function was found to be preserved in ceria nanoparticle-treated rats, demonstrating that reducing ROS levels in the retina by using ceria nanoparticles is an effective approach for treating retinal degenerative diseases.

1.5 Ceria nanoparticles for cancer therapy

Elevated levels of ROS in most cancer cells have been thought to be closely associated with many cancer-related processes, such as tumorigenesis, proliferation, and metastasis.[14] However, excessively high levels of ROS are detrimental to the cancer cells themselves by inducing apoptosis, not to mention to the normal cells.[14] This explains why cancer cells also express increased levels of antioxidant proteins to

maintain their delicate intracellular redox homeostasis. Such a double-sided role of ROS in cancer suggests that the modulation of ROS levels or the redox state using ceria nanoparticles can be an effective strategy for anticancer therapy. It is worth noting that ceria nanoparticles can work in different capacities. For example, dextran-coated ceria nanoparticles were used as a prooxidant to inhibit tumor growth and invasion of melanoma in vitro and in vivo by inducing ROS-mediated apoptosis.[15] The prooxidant activity could be promoted selectively in melanoma cells due to the tumor microenvironment, while no increase of ROS was observed in human dermal fibroblasts. Another study, on the other hand, reported the use of ceria nanoparticles as an antioxidant, where significantly reduced production of ROS suppressed the angiogenesis of ovarian cancer cells and inhibited the tumor growth in an in vivo mouse model.[16]

Ceria nanoparticles can also act as a radiation sensitizer for cancer cells as demonstrated in a pancreatic cancer radiation therapy.[17] The study showed that the low-pH condition of the cancer cells promoted the superoxide dismutase-mimetic activity of ceria nanoparticles over catalase-mimetic activity. As a result, pretreatment with ceria

nanoparticles enhanced the production of radiationinduced ROS, leading to the apoptosis of tumor cells and inhibited tumor growth.

Most of the contents of this chapter were published in the article, "Large-Scale Synthesis and Medical Applications of Uniform-Sized Metal Oxide Nanoparticles." (*Advanced Materials* **2018,1704290)

1.6 References

[1] T. Finkel, N. J. Holbrook, *Nature* **2000**, *408*, 239.

[2] A. Karakoti, S. Singh, J. M. Dowding, S. Seal, W. T. Self, *Chemical Society Reviews* **2010**, *39*, 4422.

[3] I. Celardo, J. Z. Pedersen, E. Traversa, L. Ghibelli, *Nanoscale* **2011**, *3*, 1411.

[4] A. S. Karakoti, S. Singh, A. Kumar, M. Malinska, S. V. Kuchibhatla, K. Wozniak, W. T. Self, S. Seal, *Journal of the American Chemical Society* **2009**, *131*, 14144.

[5] B. C. Nelson, M. E. Johnson, M. L. Walker, K. R. Riley, C. M. Sims, *Antioxidants* **2016**, *5*, 15.

[6] S. Das, J. M. Dowding, K. E. Klump, J. F. McGinnis, W. Self, S. Seal, *Nanomedicine* **2013**, *8*, 1483.

[7] K. J. Barnham, C. L. Masters, A. I. Bush, *Nature reviews Drug discovery* **2004**, *3*, 205.

[8] M. T. Lin, M. F. Beal, *Nature* **2006**, *443*, 787.

[9] H. J. Kwon, M.-Y. Cha, D. Kim, D. K. Kim, M. Soh, K. Shin, T. Hyeon, I. Mook-Jung, *ACS nano* **2016**, *10*, 2860.

[10] C. Allen, U. Bayraktutan, *International journal of stroke* **2009**, *4*, 461.

[11] C. K. Kim, T. Kim, I. Y. Choi, M. Soh, D. Kim, Y. J. Kim, H. Jang, H. S. Yang, J. Y. Kim, H. K. Park, S. P. Park, S. Park, T. Yu, B. W. Yoon, S. H. Lee, T. Hyeon, *Angewandte Chemie-International Edition* **2012**, *51*, 11039.

[12] S. G. Jarrett, M. E. Boulton, *Molecular aspects of medicine* **2012**, *33*, 399.

[13] J. Chen, S. Patil, S. Seal, J. F. McGinnis, *Nature Nanotechnology* **2006**, *1*, 142.

[14] M. Valko, C. Rhodes, J. Moncol, M. Izakovic, M. Mazur, *Chemico-biological interactions* **2006**, *160*, 1.

[15] L. Alili, M. Sack, C. von Montfort, S. Giri, S. Das, K. S. Carroll, K. Zanger, S. Seal, P. Brenneisen, *Antioxidants & redox signaling* **2013**, *19*, 765.

[16] S. Giri, A. Karakoti, R. P. Graham, J. L. Maguire, C. M. Reilly, S. Seal, R. Rattan, V. Shridhar, *PloS one* **2013**, *8*, e54578.

[17] M. S. Wason, J. Colon, S. Das, S. Seal, J. Turkson, J. Zhao, C. H. Baker, *Nanomedicine: Nanotechnology, Biology and Medicine* **2013**, *9*, 558.

Chapter 2. Mitochondria-targeting ceria nanoparticles as antioxidants for Alzheimer's disease

2.1 Introduction

Alzheimer's disease (AD) is one of the most common types of dementia and affects approximately 10% of people aged 65 years or more. The major pathological indicators of AD comprise the accumulation of amyloid beta (Aβ) plaques and neuro fibrillary tangles in the brain.[1,2] Although numerous studies imply the presence of crosstalk between Aβ and various molecular signaling pathways, the exact mechanism how Aβ potentiates AD pathogenesis has not been fully elucidated yet.[3-6] Additionally, Aβ-induced mitochondrial dysfunction also has been known to be a possible cause of AD through abnormal production of reactive oxygen species (ROS), such as superoxide anion, hydroxyl radical, and hydrogen peroxide.[7,8] Mitochondria are elongated membrane organelles that are found in the cytoplasm of cells and have a diameter and a height of 0.5−1 μm and 1−10 μm, respectively. Mitochondria supply cells with adenosine triphosphate (ATP) through an

oxidative phosphorylation process to maintain cellular energy homeostasis. ROS byproducts generated during this process can cause mitochondrial dysfunctions, such as DNA mutation and promotion of intrinsic apoptosis pathways.[9-11] Although the molecular basis of the impaired mitochondrial functions in AD is still far from being comprehended, several previous studies revealed that the production of ROS is involved with the interactions of Aβ peptides in mitochondria with resident proteins, such as cyclophilin D, alcohol dehydrogenase, and ATP synthase.[12-14] Since this kind of ROS-induced mitochondrial dysfunction precedes the Aβ plaque buildup in the brain, the hallmark of AD,[15,16] therapeutic agents that can protect mitochondria against oxidative stress from ROS would be very useful for the prevention and early stage treatment of AD. For example, some mitochondria-specific antioxidants, including MitoQ and SS31, are known to work effectively against AD-related oxidative stress and synaptic dysfunctions.[17-19] Ceria (CeO_2) nanoparticles less than 5 nm are known to exhibit ROS-scavenging activity in a recyclable way by reversible binding of oxygen atoms and shuttling between the Ce^{3+} (reduced) and Ce^{4+} (oxidized) states on their surface.[20-22] They have been successfully applied to protect cells against superoxide and hydrogen peroxide, which are two

predominant forms of ROS, using their superoxide dismutase-mimetic and catalase-mimetic activities, respectively.[20-22] Various therapeutic potentials of the ceria nanoparticles also have been demonstrated for neuro- and cardio-protection, wound healing, and treatment of chronic inflammation, cancer, and ocular disorders.[23-27] In particular, small ceria nanoparticles (<5 nm) showed enhanced therapeutic efficiency due to their large surface-to-volume ratio.[20] For example, 3-nm ceria nanoparticles have been shown to protect the brain against ischemic stroke in rats.[27] Here, I describe the design and synthesis of triphenylphosphonium-conjugated ceria nanoparticles (TPP-ceria NPs) that localize to mitochondria and suppress neuronal death in a 5XFAD transgenic AD mouse model. TPP is a lipophilic cation that is capable of targeting mitochondria by taking advantage of negative mitochondrion membrane potential.[28-30] The TPP-ceria NPs mitigate the reactive gliosis and morphological mitochondria damage observed in the mouse model. Altogether, our data indicate that the TPP-ceria NPs are a potential therapeutic candidate for treating mitochondrial oxidative-stress-induced damage in AD.

2.2 Experimental Section

2.2.1 Synthesis of Ceria NPs.

Ceria NPs were formed by hydrolytic sol−gel reactions. Briefly, 0.43 g of cerium(III) acetate (1 mmol) and 3.25 g of oleylamine (12 mmol) were dissolved in 15 mL of xylene. The mixture solution was stirred vigorously for 12 h at room temperature and then heated to 90 °C with a heating rate of 2 °C/min under vacuum. Deionized water (1 mL) was rapidly injected into the heated solution to initiate the sol−gel reaction, as indicated by a color change from purple to cloudy yellow. The reaction solution was then incubated at 90 °C for 3 h until it became transparent, and then was cooled to room temperature. Ceria NPs were precipitated by adding 100 mL of acetone, harvested by centrifugation, and then resuspended in chloroform to a final concentration of 10 mg/mL. I measured the size of total 591 ceria nanoparticles in three TEM images. The average size was 3.0 ± 0.8 nm.

2.2.2 Synthesis of DSPE-PEG-TPP and FITC-Conjugated DSPE-PEG.

3-CTPP (8.6 mg, 20 μmol), N-(3-(dimethylamino)propyl)-N′-ethylcarb-odiimide hydrochloride (EDCI, 11.5 mg, 60 μmol), N-hydroxysuc-

cinimide (NHS, 6.9 mg, 60 μmol), and triethylamine (20 μL) were dissolved in 1 mL of chloroform. The solution was stirred vigorously for 2 h at room temperature. Then, it was added to a second solution of 50 mg of DSPE-PEG-NH2 dissolved in 2 mL of chloroform. The solution mixture was stirred for 24 h at room temperature. The conjugation was analyzed on a MALDI TOF-TOF 5800 system installed at the National Center for Interuniversity Research Facilities (NCIRF) at Seoul National University. To produce FITC-conjugated DSPE-PEG, 7.8 mg of FITC (20 μmol), 20 μL of triethylamine, and 50 mg of DSPE-PEG-NH2 were dissolved in 10 mL of chloroform, and the solution was stirred vigorously for 24 h at room temperature.

2.2.3 Synthesis of Water-Dispersive TPP-Ceria NPs.

DSPE-PEG-TPP (25 mg) and ceria NPs (8 mg) were mixed in 25 mL of chloroform. The solution was evaporated using a rotary evaporator and dried under vacuum at 80 °C for 1 h. Eight milliliters of deionized water was then added into the flask, and sonication was performed. The transparent, light-yellow suspension was filtered by a syringe filter of 0.2 μm pore size. To remove the free DSPE-PEG-TPP, I purified the TPP-ceria NPs thoroughly by treating the obtained NPs sequentially using

high-speed ultracentrifugation at 450000g for 2 h, filtration using an Amicon centrifugal filter with a cutoff molecular weight of 50 kDa, and dialysis using a Slide-A-Lyzer dialysis cassette with a 10 kDa molecular weight cutoff (Thermo, Rockford, IL, USA) for 24 h.

2.2.4 Synthesis of Water-Dispersive FITC-Conjugated TPP-Ceria NPs and FITC-Conjugated Ceria NPs.

Water-dispersive FITC-conjugated TPP-ceria and FITC-conjugated ceria NPs were obtained by the same procedures for the preparation of water-dispersive TPP-ceria and ceria NPs except that a mixture of FITC-conjugated DSPE-PEG and DSPE-PEG was used (1:50 ratio of DSPE-PEG-FITC to DSPE-PEG-TPP).

2.2.5 Synthesis of Water-Dispersive Iron Oxide, FITC-Iron Oxide, TPP-Iron Oxide, and FITC-TPP-Iron Oxide NPs.

Water-dispersive TPP-iron oxide NPs, iron oxide NPs, FITC-conjugated TPP-iron oxide NPs, and iron oxide NPs were obtained by the same procedures for the preparation of water-dispersive TPP-ceria and ceria NPs. Iron oxide NPs with 3, 10, and 18 nm size were synthesized according to the previous publication. I measured a total of 100 iron

oxide nanoparticles in one TEM images. The average sizes were 3.0 ± 0.6, 10.0 ± 0.8, and 18.0 ± 0.4 respectively.

2.2.6 SOD Activity Assay and Catalase Activity Assay.

The superoxide scavenging activity was assessed using a SOD assay kit (Sigma-Aldrich). First, ceria NPs and TPP-ceria NPs were diluted in 200 μL of WST-1 (water-soluble tetrazolium salt, (2-(4-iodophenyl)3-(4-nitrophenyl)-5-(2,4-disulfo-phenyl)-2H-tetrazolium, monosodium salt) to get NP solutions with cerium concentrations of 0, 0.093, 0.187, 0.375, 0.75, and 1.5 mM, and the resulting NP solutions were added to each well in triplicate. SOD coupling reactions were initiated by the addition of 20 μL of xanthine oxidase solution and incubated at 37 °C for 20 min. Absorbance at 450 nm, which is proportional to SOD activity, was read using a microplate reader (Victor X4, PerkinElmer, Waltham, MA, USA). An amount of 50 U/mL SOD was defined as the activity of the enzyme that inhibits the reduction reaction of WST-1 with superoxide anion by 50% in experiments quantifying SOD-mimetic activity. Three repeated sets of measurements were performed. The catalase activity of ceria and TPP-ceria NPs was measured by an Amplex Red hydrogen peroxide/peroxidase assay kit (Molecular Probes Inc.). In the presence

of catalase activity, Amplex Red reagent (10-acetyl-3,7-dihydroxyphenoxazine) reacts with hydrogen peroxide to yield a red fluorescent resorufin oxidation product. For this, ceria or TPP-ceria NPs were diluted in 1× reaction buffer containing 100 μM Amplex Red reagent and 2 mM hydrogen peroxide, with different cerium concentrations of 0, 0.25, 0.5, and 1 mM. Then, 50 μL of the above solution was added to microplate wells in triplicate. The microplate was protected from light and incubated at room temperature for 30 min. The absorbance at 490 nm was then measured with a microplate reader. One mU/mL HRP worked as the 100% control when measuring the catalase-mimetic activity. All the measurements were performed in triplicate.

2.2.7 Cell Viability Assays.

SH-SY5Y and HT22 were seeded at 10000 cells per well in a 96-well plate and cultured for 24 h. Ceria or TPP-ceria NPs were diluted in cell media and added to triplicate microplate wells containing increasing cerium concentrations (0, 0.125, 0.25, 0.5, and 1 mM), The microplate was incubated at 37 °C for 24 h, and 20 μL of 5 mg/mL of 3-[4,5-dimethylthialzol-2-yl]-2,5-diphenyltetrazolium bromide (MTT) was added to each well. The microplate was incubated at 37 °C for 4 h, and

then the medium was replaced with 200 μL of dimethyl sulfoxide per well. Cell viability was determined by measuring absorbance at 595 nm.

2.2.8 Mitochondrial ROS-Scavenging Activity Analysis.

SH-SY5Y, HT22, and U373 cells were seeded at 1×10^5 per well in a 24-well plate and cultured for 24 h. Ceria or TPP-ceria NPs were diluted in cell media with 0.1 mM of cerium concentrations and added to wells containing 5 μM Aβ. The plate was incubated at 37 °C for 12 h, at which point the medium was removed and cells were incubated with 1 mL of 5 μM MitoSOX cell media at 37 °C for 10 min. Then, the cells were washed three times with DPBS, harvested by trypsinization, and fixed in 3% formaldehyde for 10 min. Fixed cells were collected by centrifugation and resuspended in 0.5 mL of PBS for flow cytometry analysis on an Accuri C6 flow cytometer (BD Biosciences, Franklin Lakes, NJ, USA) with a 473 nm laser and 575 nm filter. Relative mitochondrial ROS-scavenging activity was determined by the fluorescence intensity of MitoSOX.

2.2.9 Nanoparticle Subcellular Localization.

SH-SY5Y and HeLa cells (1×10^5) were seeded in 2 mL of media in a confocal dish and incubated for 24 h. The media were then replaced with

2 mL of media containing 0.5 μM MitoTracker Orange CMTMRos (Invitrogen-Life Technologies, Carlsbad, CA) and 0.5 μM LysoTracker Blue DND-22 (Invitrogen-Life Technologies, Carlsbad, CA) for 30 min at 37 °C. Cells were washed three times with DPBS and then cultured in cell media containing FITC-conjugated ceria or TPP-ceria NPs and 1 mM cerium at 37 °C for 12 h. NP movement and subcellular localization were monitored by confocal microscopy with an LSM-780 microscope (Carl Zeiss, Oberkochen, Germany). Colocalization coefficients were obtained by analyzing the microscopic images with ZEN2012 software (Carl Zeiss, Oberkochen, Germany).

2.2.10 Animal Model.

The 5XFAD transgenic mouse model develops severe amyloidal plaques and exhibits an AD-like phenotype. For our analyses, 5XFAD mice overexpressing the human amyloid precursor protein 695 isoform (APP695) harboring three familial AD (FAD) mutations (Swedish: KM670/671NL; Florida: I176 V, and London: V717I) and human presenilin 1 (PSEN1) containing the M146L and L286 V mutations under the transcriptional control of the mouse Thy1 promoter were purchased

from Jackson Laboratories (Bar Harbor, ME, USA). Six month old 5XFAD and B6/SJL littermate control mice were used for tissue analysis.

2.2.11 Stereotaxic Injections.

Wild-type + saline (LT + sham), transgenic + saline (Tg + sham), and Tg + FITC-conjugated TPP-ceria NPs (Tg + TPP-ceria) treatment mice groups (4 months old) were anesthetized with isofluorane and placed in a stereotaxic frame (myNeuroLab, St. Louis, MO, USA). Unilateral subicular injections (−4.16 mm AP, 3.25 mm ML, and −4.0 mm DV) of saline or TPP-ceria NPs were performed using a stereotaxic apparatus, as described by the Paxinos and Watson atlas. Mice were injected with saline or TPP-ceria NPs using a Hamilton microsyringe (3 μL, 0.5 μL/min, 26 gauge syringe). To examine the therapeutic effects of TPP-ceria, immunofluorescence and biochemical analyses were performed 2 months after surgery. Animal treatment and maintenance were approved by the Ethics Review Committee for Animal Experimentation in Seoul National University.

2.2.12 Immunostaining.

Mice were anesthetized with a mixture of Zoletil (Virbac, Carros, France) and Rompun (Bayer Korea, Seoul, Korea) and perfused with 4%

paraformaldehyde solution in PBS. Brains were subsequently fixed in 0.1 M phosphate buffer containing 4% paraformaldehyde for 20 h at 4 °C and incubated in a 30% sucrose solution in 0.05 M PBS for 72 h prior to sectioning into 30 μm slices using a freezing cryostat (Leica, Wetzlar, Germany). For immunolabeling, tissue sections were incubated at 4 °C overnight with anti-NeuN antibody (1:1000; Millipore, Billerica, MA, USA), anti-GFAP antibody (1:1000; Invitrogen, Carlsbad, CA, USA), and anti-Iba1 antibody (1:500; Wako, Tokyo, Japan). For Aβ immunofluorescence, tissue sections were pretreated with 70% formic acid for 20 min prior to incubation with biotin-labeled 4G8 antibody (1:2000; Covance, Princeton, NJ, USA). Stained tissue sections were then incubated with Alexa 594-conjugated streptavidin, donkey anti-mouse Alexa 594, goat anti-rat Alexa 594, and goat anti-rabbit Alexa 647 (all 1:500; Molecular Probes) for 1 h at room temperature and counterstained with 4′-6diamidino-2-phenylindole (DAPI, 1:5000; Sigma-Aldrich) for 10 min prior to imaging.

2.2.13 Quantification of Immunoreactivity.

For quantification of immunoreactivity, three sections (100 nm apart) from each mouse brain were taken from similar regions. Five random

acquisition areas were considered for each brain section. Stained NeuN-positive cells were counted using Image-Pro Plus (Media Cybernetics, Bethesda, MD, USA). To quantify biotin-4G8, GFAP, and Iba-1-positive area, the immunofluorescence region in the subiculum areas was analyzed using the ImageJ software (National Institutes of Health, USA).

2.2.14 Quantification of Cerium Ion Concentration after Administration of TPP-Ceria NPs in Brain Tissue.

Determination of cerium content in the contralateral and ipsilateral side of the brain was performed by inductively coupled plasma mass spectrometry analysis (ELAN 6100, PerkinElmer SCIEX). Brain tissue was dissolved in aqua regia. The resulting solutions were diluted in HNO_3 (2%, 2 ppb, 1:300 v/v). Elemental analysis was performed using an inductively coupled plasma mass spectrometer (ELAN 6100, PerkinElmer).

2.2.15 Preparation and Imaging the Brain Tissue Using TEM.

Brain tissues from 5XFAD mice were sequentially fixed overnight in a mixture of cold 2.5% glutaraldehyde in 0.1 M phosphate buffer (pH 7.2) and 2% paraformaldehyde in 0.1 M phosphate or cacodylate buffer (pH 7.2) before being embedded in epoxy resin. The embedded samples were

loaded into capsules and polymerized at 38 °C for 12 h and then at 60 °C for 48 h. Thin sections were made using an ultramicrotome (RMC MT-XL; RMC Products, Portsmouth, NJ, USA) and collected on a copper grid. Appropriate areas for thin sectioning were cut to 65 nm thickness and stained with saturated 4% uranyl acetate/4% lead citrate prior to TEM before examination with a transmission electron microscope (JEM-1400, JEOL) at 80 kV.

2.2.16 Statistical Analysis.

Quantitative data were analyzed statistically with Student's t tests or ANOVA by Prism 6 (GraphPad, San Diego, CA, USA).

2.3 Result and Discussion

2.3.1 Synthesis and Characterization of TPP-Ceria Nanoparticles. Two sets of biocompatible ceria nanoparticles were synthesized using a modified reverse micelle method,[27,31] and transferred to water by coating with either 1,2-distearoyl-snglycero-3-phosphoethanolamine-N-[methoxy(po -lyethylene glycol)-2000] (DSPE-PEG) (designated as ceria NPs) or TPP-conjugated 1,2-distearoyl-sn-glycero-3-phosphoethanolamine-N-[amino(polyethylene glycol)-2000] (DSPE-PEG-TPP) (designated as TPP-ceria NPs), which was obtained by conjugating carboxyl group of (3-carboxypropyl) triphenylphosphonium bromide (3-CTPP) with an amine group in DSPE-PEG-NH2 (Figure 2.1a and Figures 2.2−2.4). Transmission electron microscopy (TEM) reveals uniform nanoparticles with a 3 nm core diameter (Figure 2.1b). After transfer to water, hydrodynamic diameter and ζ-potential of ceria and TPP-ceria NPs increase from 11 to 22 nm and change from −23 to 45 mV, respectively. The observed size and surface potential changes confirm the successful conjugation of TPP onto the nanoparticles (Figure 2.1c, d and Figure 2.5). The hydrodynamic diameters of the TPP-ceria

NPs in phosphate buffered saline (PBS), Dulbecco's modified Eagle's medium (DMEM) with 10% fetal bovine serum (FBS), and human blood plasma are monitored for 1 month. The measured hydrodynamic diameters in those three different media remain almost constant during the period, ~24 ± 3, ~23 ± 2, and ~26 ± 2 nm in PBS, DMEM with 10% FBS, and human blood plasma, respectively (Figure 2.6), indicating good colloidal stability of the TPP-ceria NPs in physiological conditions.

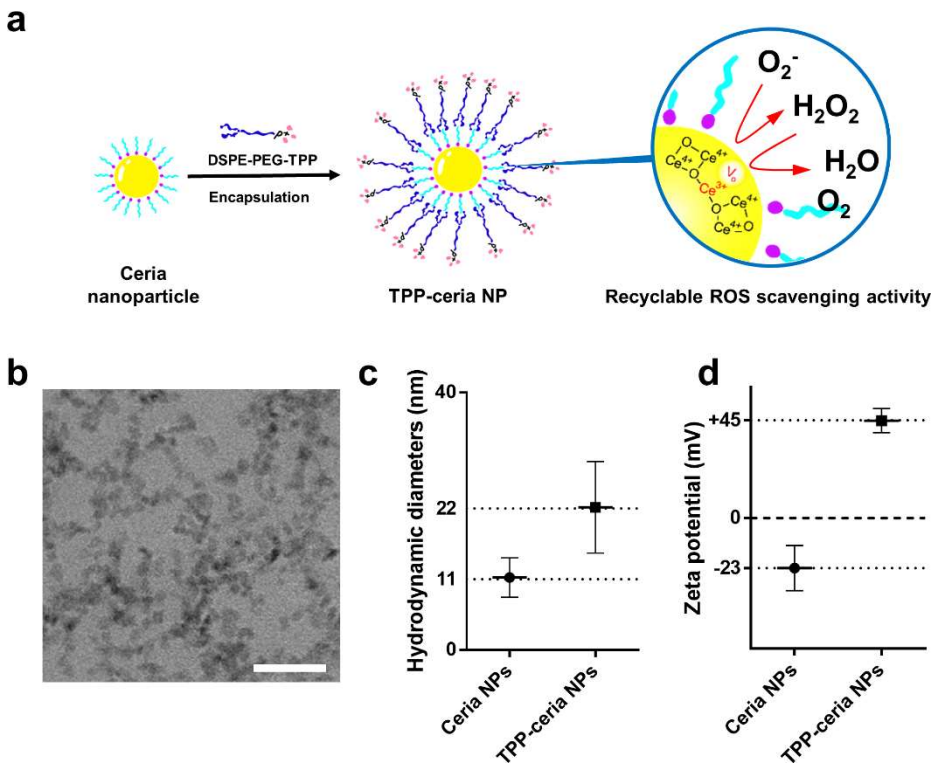

Figure 2.1. Design, synthesis, and characterization of TPP-ceria nanoparticles as a therapeutic mitochondrial antioxidant for Alzheimer's disease. (a) DSPE-PEG-TPP-coated ceria nanoparticles exhibiting ROS recyclable scavenging activity. (b) TEM image of TPP-ceria NPs (scale bar = 20 nm). (c,d) Hydrodynamic diameters and ζ-potentials of ceria and TPP-ceria NPs. Error bars represent standard deviation

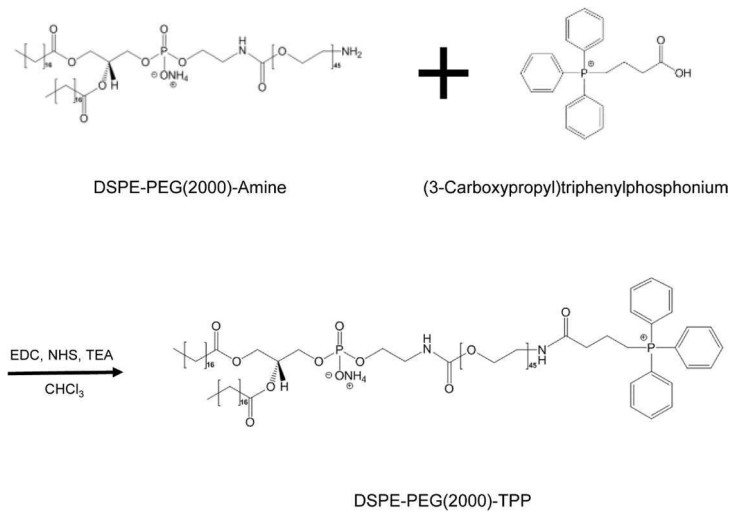

Figure 2.2. Scheme of DSPE-PEG-amine-TPP conjugation. Triphenylphosphonium (TPP) was chemically conjugated to DSPE-PEG-amine by EDC coupling.

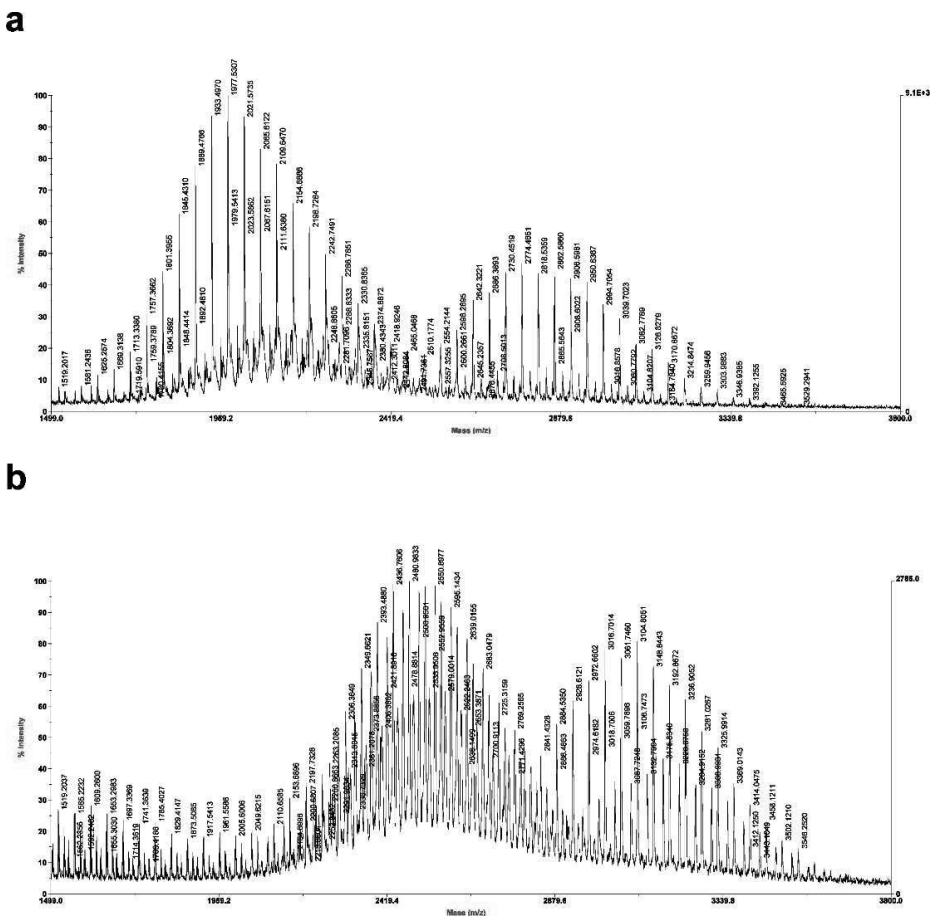

Figure 2.3. MALDI-TOF spectra of DSPE-PEG-TPP. The molecular weight of DSPE-PEG increased following conjugation with TPP. Molecular weight of TPP is 349.39 g/mol. The increased molecular weight of main peak is approximately 350 g/mol.

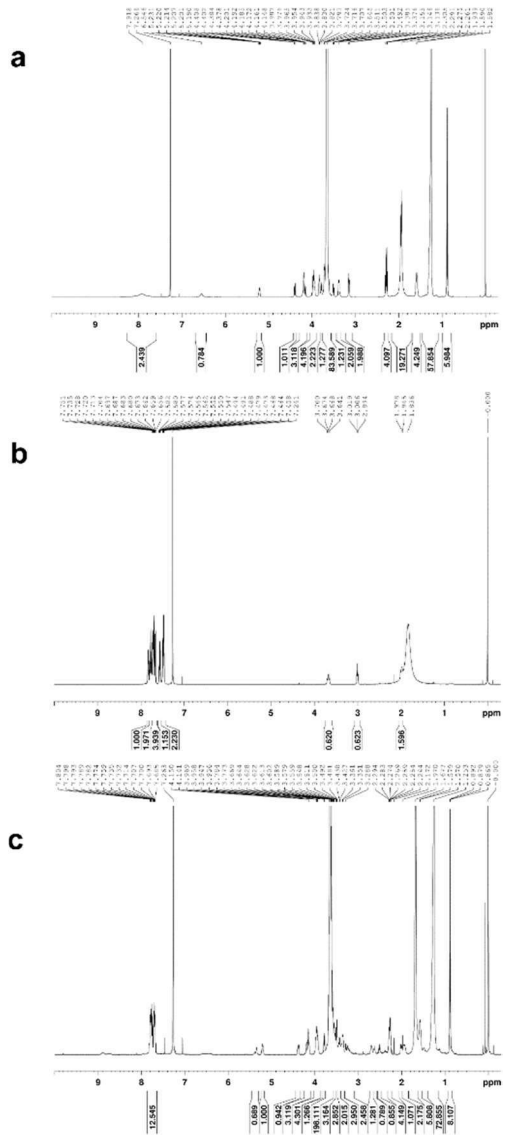

Figure 2.4. NMR spectra of DSPE-PEG-amine, TPP and DSPE-PEG-TPP. A) DSPE-PEG-amine, B) TPP, C) DSPE-PEG- TPP.

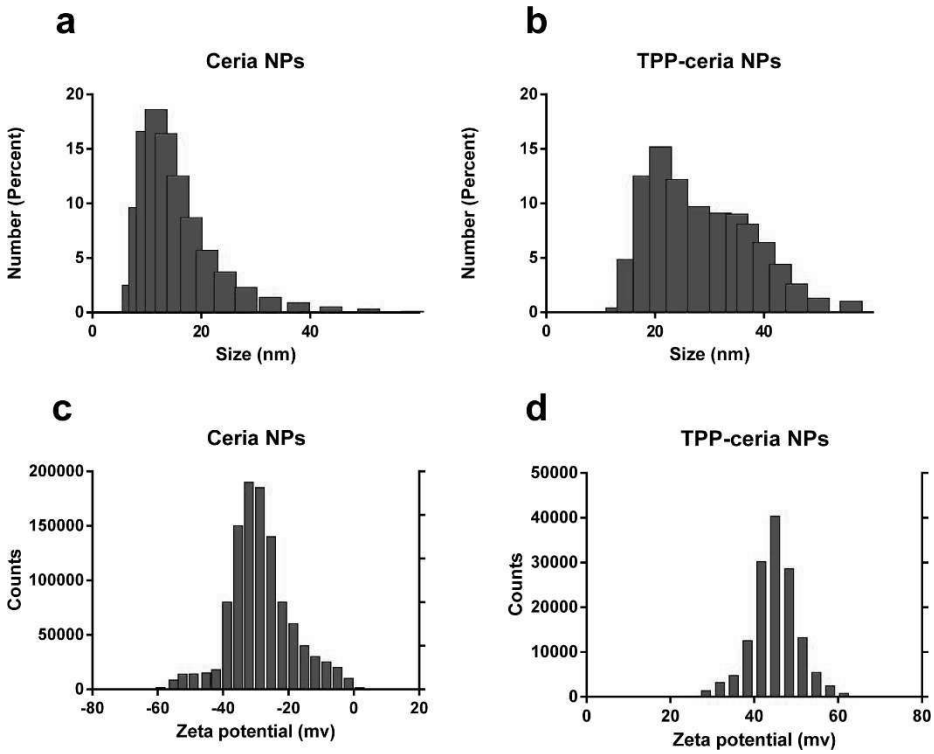

Figure 2.5. DLS spectra of ceria NPs and TPP-ceria NPs. A) Hydrodynamic diameters of ceria NPs, B) Hydrodynamic diameters of TPP-ceria NPs, C) Zeta potential of ceria NPs, D) Zeta potential TPP-ceria NPs.

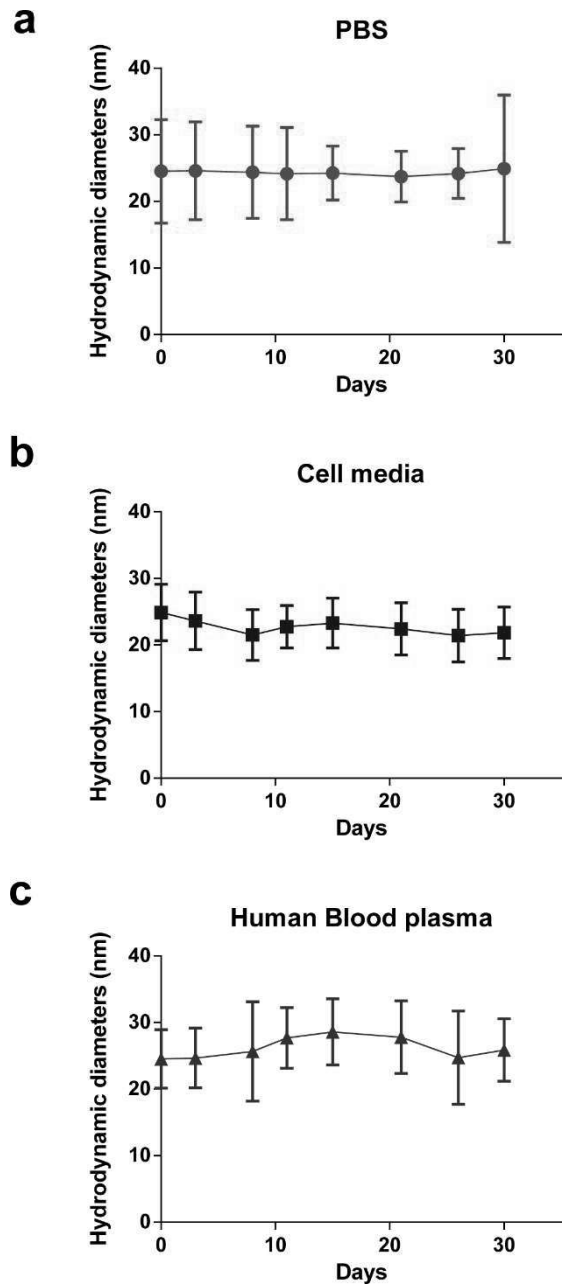

Figure 2.6. Hydrodynamic diameters of TPP-ceria NPs in A) PBS, B) Cell media (DMEM+10% FBS), C) Human blood plasma.

2.3.2 Cellular and Mitochondrial Uptake of TPP-Ceria Nanoparticles.

I studied the effect of nanoparticle size, surface coating, and surface charge on cellular and mitochondrial uptake profile of the TPP-ceria NPs. To visualize the nanoparticles under a confocal fluorescence microscope, I first synthesized fluorescein isothiocyanate (FITC)-conjugated DSPE-PEG (DSPE-PEG-FITC) and used it with a mass ratio of 1:50 DSPE-PEG-FITC to DSPE-PEG-TPP to produce FITC-conjugated nanoparticles. To investigate the effect of hydrodynamic size, I prepared FITC-conjugated TPP-ceria NPs (FITC-TPP-ceria NPs) with different hydrodynamic sizes by varying the mass ratio of DSPE-PEG-TPP and DSPE-PEG-FITC to ceria NPs. When I use 3:1, 2:1, 1:1, 0.5:1, and 0.25:1 ratios, the produced FITC-TPP-ceria NPs show hydrodynamic diameters of 22, 30, 43, 51, and 57 nm and ζ-potentials of 44, 41, 49, 48, and 39 mV, respectively (Figure 2.7). The hydrodynamic diameter of the FITC-TPP-ceria NPs increases as the relative amount of DSPE-PEG-TPP and DSPE-PEG-FITC decreases. In experiments using SH-SY5Y and HeLa cells, I observed that the FITC-TPP-ceria NPs obtained with a mass ratio of 3:1 are localized to mitochondria, while the FITC-TPP-ceria NPs obtained with lower mass ratios of 1:1 or 0.5:1 are localized

mostly to lysosome (Figure 2.8). For the latter case, several ceria nanoparticles seem to be associated together, resulting in the increased hydrodynamic diameter. Those FITC-TPP-ceria NPs with larger hydrodynamic diameter show low colloidal stability and tend to be aggregated in physiological conditions. Therefore, they cannot be delivered into mitochondria and are captured by lysosome despite their positive surface charge of TPP. These results suggest that both small hydrodynamic diameter and good colloidal stability of TPP-ceria NPs play a key role in mitochondrial-targeting strategy. As a result, only TPP-ceria NPs with a hydrodynamic diameter of 22 nm can penetrate mitochondria efficiently. I also examined the effect of nominal size of the core nanoparticles. Since the size of the ceria NPs (3 nm) is not readily controllable in our current synthetic method, I synthesized iron oxide nanoparticles instead as a core material because their size control is much easier.[32] Specifically, I synthesized FITC-conjugated TPP-iron oxide NPs (FITCTPP-iron oxide NPs) with three different core sizes (3, 10, and 18 nm) to investigate the effect of the core nanoparticle size on the cellular and mitochondrial uptake. I also prepared the FITC-iron oxide NPs with the same core size and without TPP conjugation. Their hydrodynamic sizes are 27, 31, and 41 nm for FITC-TPP-iron oxide NPs

and 20, 27, and 37 for FITC-iron oxide NPs without TPP conjugation, for the core sizes of 3, 10, and 18 nm, respectively. ζ-Potentials are measured as 45, 47, and 60 mV for the FITC-TPP-iron oxide NPs and −35, −37, and −44 mV for those without TPP conjugation, for the core sizes of 3, 10, and 18 nm, respectively (Figure 2.7). I observe that FITC-TPP-iron oxide NPs with core sizes of 3 or 10 nm are localized to mitochondria, while all the other types of FITC-iron oxide nanoparticles (18 nm TPP-iron oxide NPs and iron oxide NPs without TPP conjugation regardless of the core size) remain mostly in cytoplasm in SH-SY5Y and HeLa cells (Figures 2.9). Similar to ceria NPs, FITC-iron oxide NPs with a 3 nm core are found in cytoplasm due to the absence of TPP. FITC-TPP-iron oxide NPs with a 3 nm core can penetrate into mitochondria because of their similar core size, hydrodynamic diameter, and ζ-potential to TPP-ceria NPs. Interestingly, FITC-TPP-iron oxide NPs with a 10 nm core also can be delivered to mitochondria efficiently, while those with an 18 nm core cannot, suggesting that large nanoparticles are hard to cross the mitochondria membrane even if they have a hydrophobic layer and a positive surface charge of TPP. Our data indicate that small core size (3 and 10 nm) is another key feature in our mitochondria-targeting approach. To explore the effect of the surface

charge and coating, I also synthesized FITC-conjugated amino-ceria NPs using DSPE-PEG-NH2. The resulting FITC-conjugated amino-ceria NPs exhibit a positive ζ-potential (+38 mV), which is similar to that of the FITC-TPP-ceria NPs (+45 mV). I also prepared negatively charged FITC-conjugated carboxylic ceria NPs (−21mV) using DSPE-PEG-COOH. The hydrodynamic diameters of the FITC-conjugated amino- and carboxylic-ceria NPs are 26 and 28 nm, respectively (Figure S6). Although the measured hydrodynamic diameters are similar to those of FITC-TPP-ceria NPs (22 nm) and FITC-TPP-iron oxide NPs with core sizes of 3 or 10 nm (27 and 31 nm), both the FITC-conjugated amino- and carboxylic-ceria NPs are found mainly in cytoplasm of SH-SY5Y and HeLa cells regardless of their surface charge (Figure 2.10). The overall distribution of FITC-amino and FITC-carboxylic-ceria NPs in cells is similar to that of nontargeted ceria NPs. It is noteworthy that amine groups in FITC-amino-ceria NPs are hydrophilic, and thus the NPs cannot be delivered to mitochondria even though they have ζ-potential similar to that of TPP-ceria NPs. Therefore, it can be inferred that hydrophobicity of TPP is critical for the mitochondrial-targeting application. In summary, the key features of our TPP-ceria NPs for mitochondria targeting are small core size (3 nm), small hydrodynamic

diameter (22 nm), good colloidal stability, positive ζ-potential (+45 mv), and hydrophobicity.

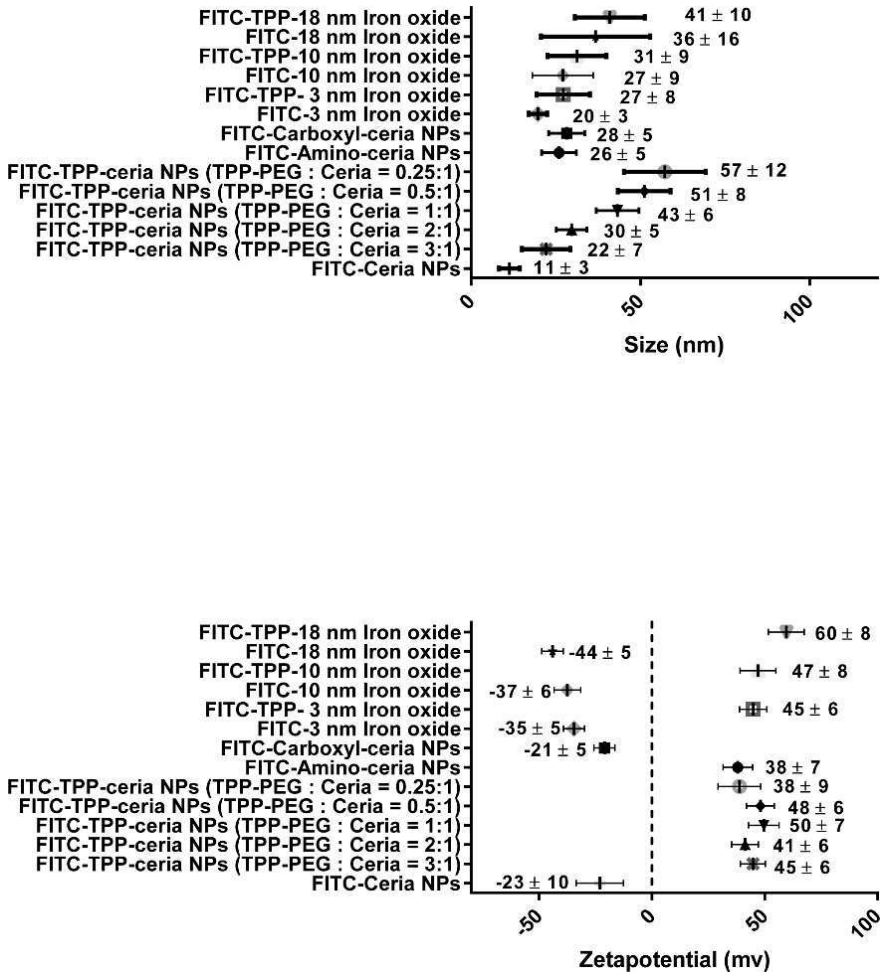

Figure 2.7. Hydrodynamic diameters and zeta potentials of FITC conjugated TPP-ceria NPs, iron oxide NPs, carboxyl-ceria NPs, amino-ceria NPs and ceria NPs. a) Hydrodynamic diameters of FITC conjugated TPP-ceria NPs, iron oxide NPs, carboxyl-ceria NPs, amino-ceria NPs and ceria NPs. b) zeta potentials of FITC conjugated TPP-ceria NPs, iron oxide NPs, carboxyl-ceria NPs, amino-ceria NPs and ceria NPs.

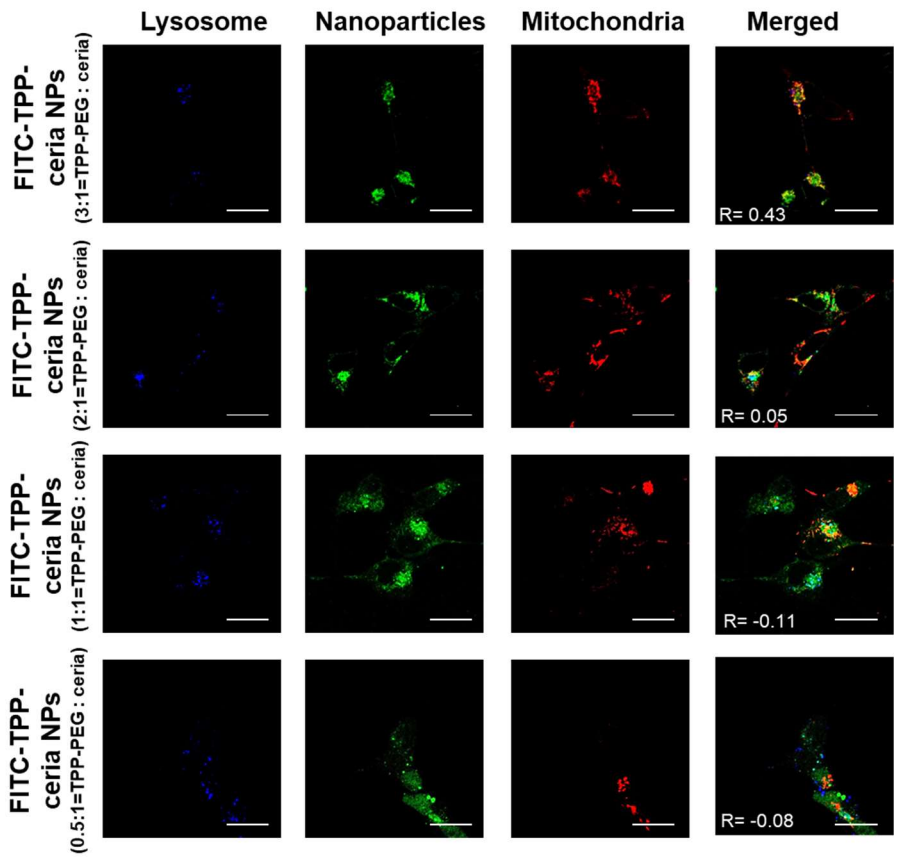

Figure 2.8. Representative confocal fluorescence microscopy images showing the subcellular colocalization of FITC-conjugated TPP-ceria with different mass ratio of TPP-DSPE-PEG to ceria NPs (green) in SH-SY5Y. SH-SY5Y cells were stained with LysoTracker (blue) and MitoTracker (red). Colocalization of FITC-conjugated TPP-ceria NPs and mitochondria (red) is shown in merged images (scale bar = 20 μm). R is the colocalization coefficient between green and red fluorescence.

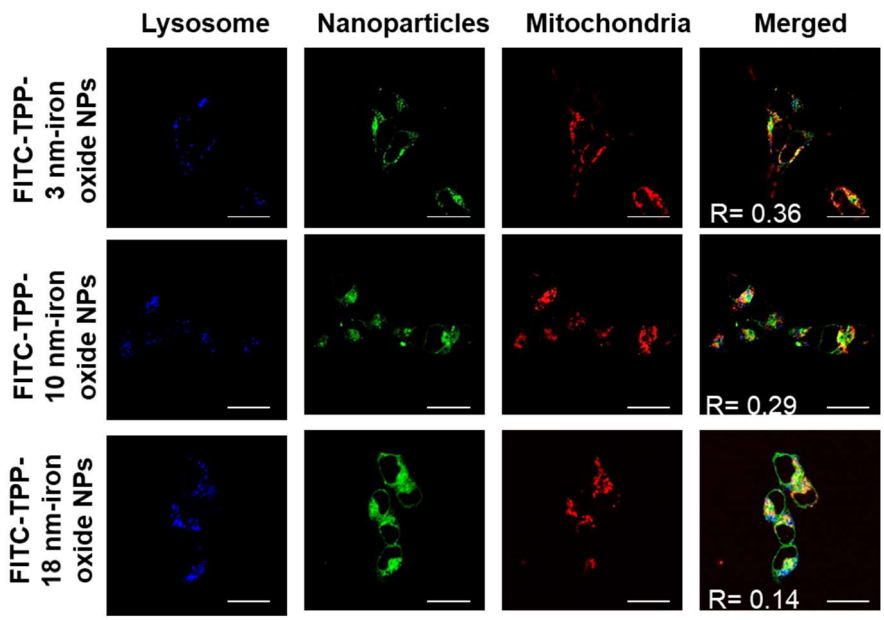

Figure 2.9. Representative confocal fluorescence microscopy images showing the subcellular colocalization of FITC-conjugated TPP-iron oxide NPs with 3 nm, 10 nm, and 18 nm core size in SH-SY5Y. SH-SY5Y cells were stained with LysoTracker (blue) and MitoTracker (red). Colocalization of FITC-conjugated TPP-iron oxide NPs and mitochondria (red) is shown in merged images (scale bar = 20 μm). R is the colocalization coefficient between green and red fluorescence.

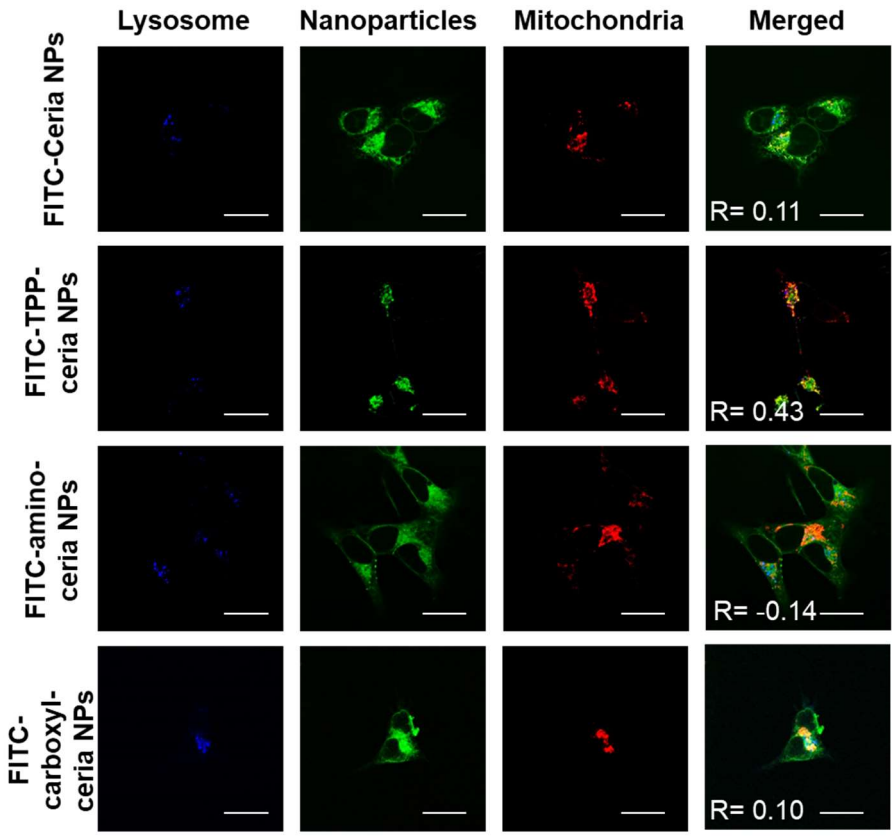

Figure 2.10. Representative confocal fluorescence microscopy images showing the subcellular colocalization of FITC-conjugated TPP-ceria, FITC-conjugated ceria NPs, FITC-conjugated carboxyl-ceria NPs and FITC-conjugated amino-ceria NPs (green) in SH-SY5Y cells. SH-SY5Y cells were stained with LysoTracker (blue) and MitoTracker (red). Colocalization of FITC-conjugated TPP-ceria NPs and mitochondria (red) is shown in merged images (scale bar = 20 μm). R is the colocalization coefficient between green and red fluorescence.

2.3.3 *In Vitro* Studies of TPP-Ceria Nanoparticles.

ROS scavenging activity of TPP-ceria NPs was evaluated by superoxide dismutase and catalase activity assays, where dose dependent activity was observed (Figure 2.11). MTT assay was performed to evaluate the cell viability of SH-SY5Y (human neuroblastoma) cells treated with TPP-ceria NPs, which show that the NPs are nontoxic at cerium ion concentrations below 0.125 mM (Figure 2.12a). The delivery of TPP-ceria NPs into mitochondria was analyzed by confocal microscopy using SHSY5Y and HeLa (human epithelial carcinoma) cells treated with FITC-TPP-ceria NPs. Significantly higher colocalization coefficient was obtained for FITC-TPP-ceria NPs with respect to mitochondria than that for FITC-ceria NPs (Figure 2.12b). It is worth noting that the mitochondrial localization of the FITCTPP-ceria NPs is observed at 2 h post-treatment and accumulation continues, whereas FITC-ceria NPs remain randomly distributed in the cell (Figure 2.12c). Based on these results, I conclude that the TPP moiety potentiates the mitochondrial localization of the TPP-ceria NPs. Since TPP-ceria NPs are predominantly targeted to mitochondria, I evaluated whether they affected Aβ-induced mitochondrial ROS accumulation in SH-SY5Y neuronal cells. Additionally, mitochondrial ROS levels were measured

by flow cytometry using MitoSOX, a cell-permeable indicator that recognizes mitochondria-specific ROS. These analyses reveal that TPP-ceria NPs markedly inhibit Aβ-induced mitochondrial ROS (Figure 2.13).

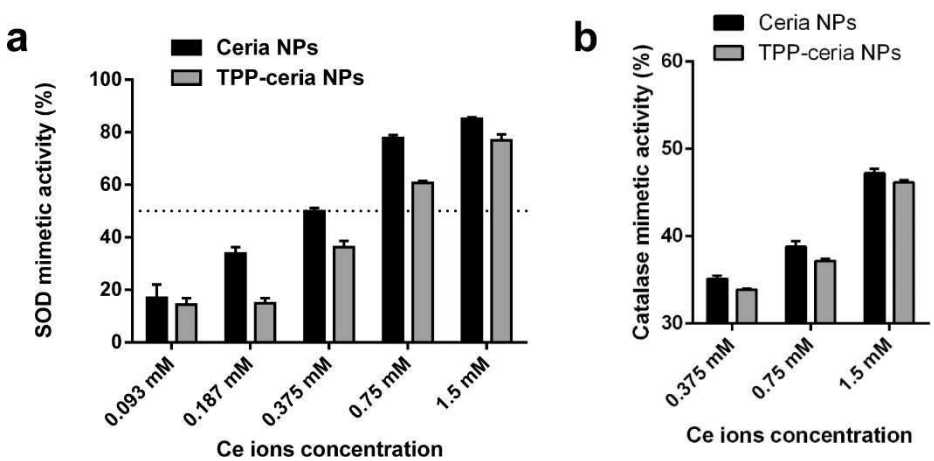

Figure 2.11. SOD and catalase mimetic activity of ceria NPs and TPP-ceria NPs. a) SOD mimetic activity (n = 9), b) Catalase mimetic activity (n = 9).

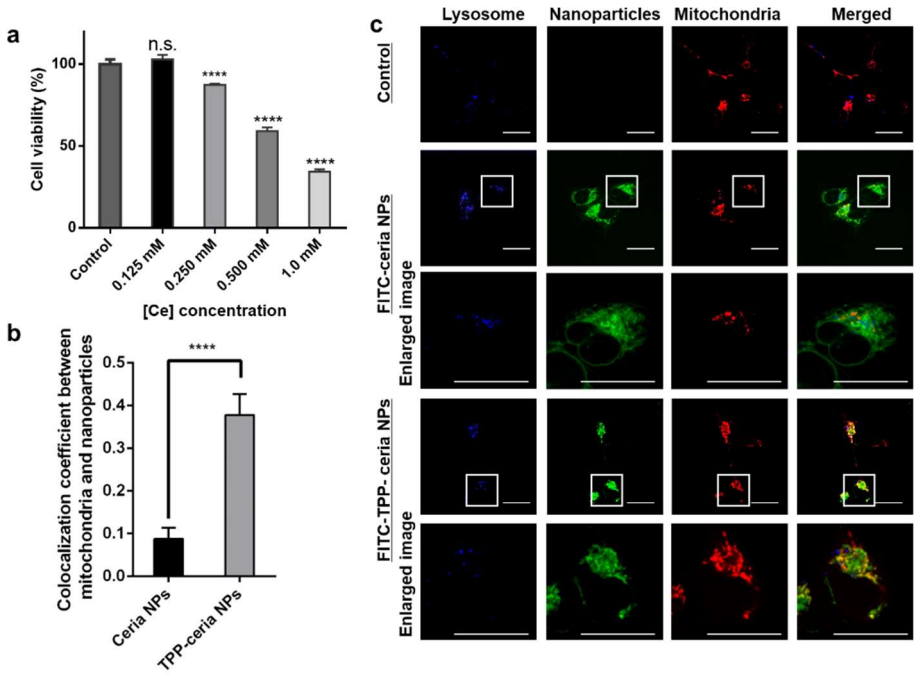

Figure 2.12 *In vitro* data of TPP-ceria NPs. (a) Cell viability of TPP-ceria NPs in SH-SY5Y cell lines after 24 hours of exposure. Statistical significance was analyzed using 1-way ANOVA test with **** marking $p < 0.0001$ and n.s. marking no significance difference ($n = 9$ per group). Error bars represent standard deviation. (b) Co-localization coefficient between mitochondria and FITC-conjugated TPP-ceria NPs and FITC-conjugated ceria NPs in in SH-SY5Y cells. Statistical significance was analyzed using Student's t-test with **** marking $p < 0.0001$. Error bars represent standard deviations ($n = 5$ per group). (c) Representative confocal fluorescence microscopy images showing the subcellular co-localization of FITC-conjugated TPP-ceria and FITC-conjugated ceria NPs. SH-SY5Y cells were stained with LysoTracker (blue) and MitoTracker (red). Co-localization of FITC-conjugated TPP-ceria/ceria NPs (green) and mitochondria is shown in merged images (scale bar = 20 μm). Magnified images of the boxed areas are shown below.

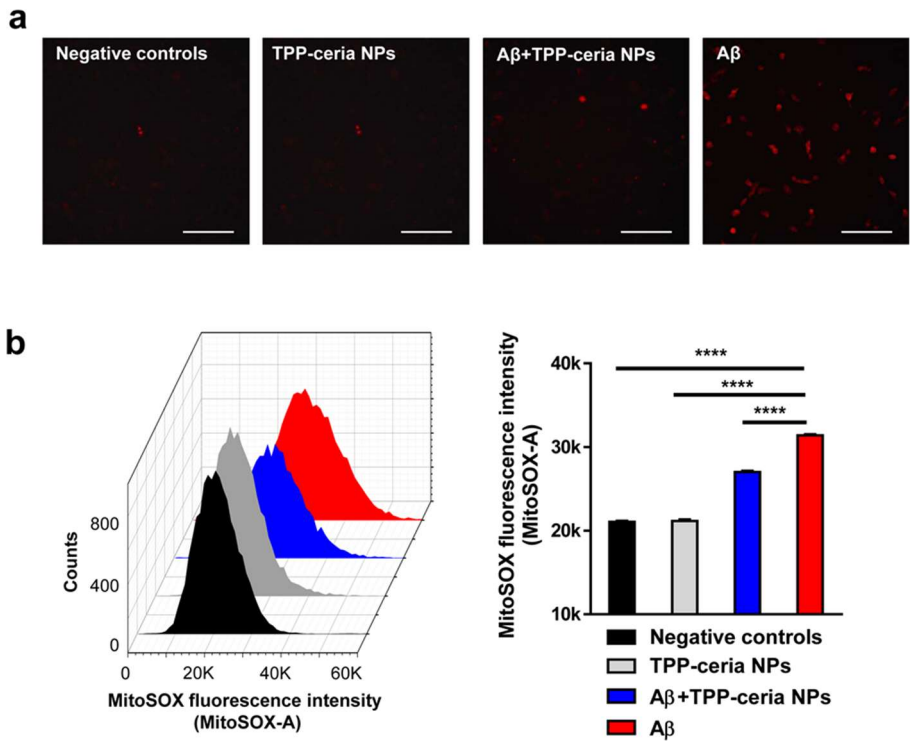

Figure 2.13. TPP-ceria NPs significantly inhibit Aβ-induced mitochondrial ROS in vitro. (a) Confocal fluorescence images of mitochondrial ROS accumulation in SH-SY5Y cells obtained by MitoSOX. SH-SY5Y cells were stained using 5 μM MitoSOX without any treatment (negative control) and after exposed to 0.1 mM TPP-ceria NPs (TPP-ceria NPs), to 5 μMAβ and 0.1 mM TPP-ceria NPs (Aβ + TPP-ceria NPs), and to 5 μMA β (Aβ) for 12 h. Scale bar = 50 μm. (b) MitoSOX fluorescence intensity measured in SH-SY5Y cells by flow cytometry. Statistical analysis was performed using an ANOVA test with **** indicating $p < 0.0001$. Error bars represent 95% confidence intervals.

2.3.4 Translocation of TPP-Ceria Nanoparticles into Mitochondria.

The mitochondrial translocation of FITC-TPP-ceria NPs in HeLa cells was also monitored by real-time confocal microscopy. Cells were stained with MitoTracker and subsequently treated with FITC-TPP-ceria NPs. The confocal microscopic images reveal that FITC-TPP-ceria NPs distribute evenly in the cells within 6 h, and their distribution eventually saturated after 10 h (Figure 2.14a). Conversely, DSPE-PEG-FITC and free FITC cannot enter the cells and remains in the culture media even after 16 h (Figure 2.14b,c). Colocalization coefficients for mitochondria and FITC-TPP-ceria NPs were calculated from the time-lapse images and reveal that colocalization increases almost linearly with time and begins to saturate after 10 h (Figure 2.14d). Since I observe that some population of the FITC-TPP-ceria NPs internalize into mitochondria quite quickly within less than 1 h, it is possible that mechanisms other than endocytosis, which usually takes longer, are involved in the cellular uptake of the FITC-TPP-ceria NPs. It has been reported that cellular uptake of various NPs can proceed via several mechanisms including cross-membrane, clathrin- and caveolae-mediated endocytosis, and macro-pinocytosis.[33-35] Although the exact uptake mechanism of the FITC-TPP-ceria NPs has not been elucidated yet, it is possible that

several mechanisms are involved together in the localization of the FITC-TPP-ceria NPs to mitochondria as can be inferred from the observed time scales ranging from less than 1 to 10 h.

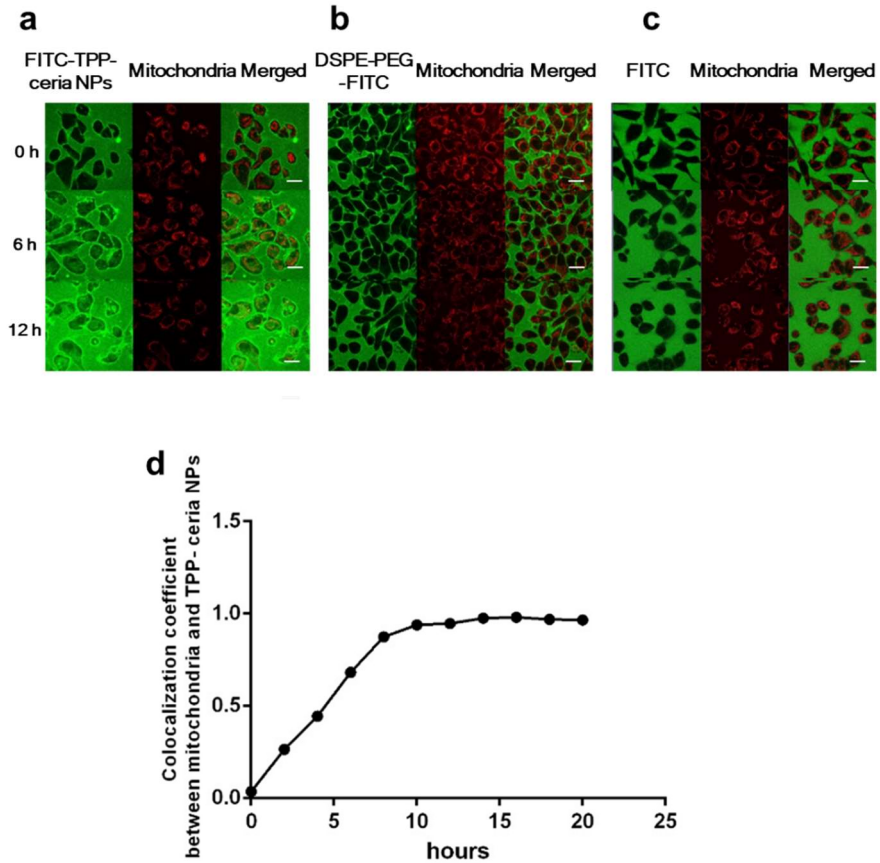

Figure 2.14. Mechanism of TPP-ceria NPs movement into mitochondria in HeLa cells. Time-serial confocal image of a) FITC conjugated TPP-ceria NPs, b) DSPE-PEG-FITC c) FITC. Scale bar = 20 μm. d) Colocalization coefficient between mitochondria and FITC conjugated TPP–ceria NPs based on Figure 2.14a.

2.3.5 Reduction of Aβ-Induced Neuronal Cell Loss.

I investigated the effect of TPP-ceria NPs in suppressing the pathogenesis of AD using the in vivo 5XFAD mouse model. Previous studies demonstrated that 5XFAD mice, a well-known AD mouse model, exhibit pathology similar to that observed in AD patients, including robust neuronal cell death and increased Aβ plaque accumulation in the subiculum.[18,36] Because nanoparticles generally cannot cross the blood−brain barrier, I stereotactically injected the FITC-TPP-ceria NPs into subicula of 5XFAD mice (Figure 2.15a).[37] The distribution of the injected FITC-TPP-ceria NPs was examined by fluorescence images at 6 months postinjection (Figure 2.15b). Immunohistochemical analysis of FITC-TPP-ceria NP-treated 5XFAD mice reveals that the NPs localize predominantly in the subicula. Inductively coupled plasma mass spectrometry analysis of the brain lysate also confirm that the delivered TPP-ceria NPs exist mostly at the injected (ipsilateral) side of the subicula (Figure 2.15c). To validate the neuro-protective effect of TPP-ceria NPs on AD pathogenesis, I examined if the injected TPP-ceria NPs can alleviate the neuronal loss observed in the brains of 5XFAD mice. For this experiment, at 2 months after NP injection, the neurons in brain slices from mice were stained with NeuN antibody, and then the positive

cells were quantified. It is evident that the administration of TPP-ceria NPs significantly restores neuronal viability of the 5XFAD mice (Figure 2.16a). Since the accumulation of Aβ, which was traced with Aβ specific antibody 4G8, did not show significant difference between the brains of TPP-ceria NP-treated and nontreated mice (Figure 2.16b), it is conceived that TPP-ceria NPs ameliorate the neuronal damage of 5XFAD mice in an indirect way, independent of the Aβ accumulation. Interestingly, some TPP-ceria NPs associate with the core of plaques that mainly consist of hydrophobic domains. Since plaques are formed by hydrophobic interaction among Aβ, our TPP-ceria NPs, which have both hydrophobic and hydrophilic parts, can bind to them through hydrophobic interactions. It is possible that van der Waals interaction is also involved in the association similarly to the complex between nanoparticles and Aβ.[38]

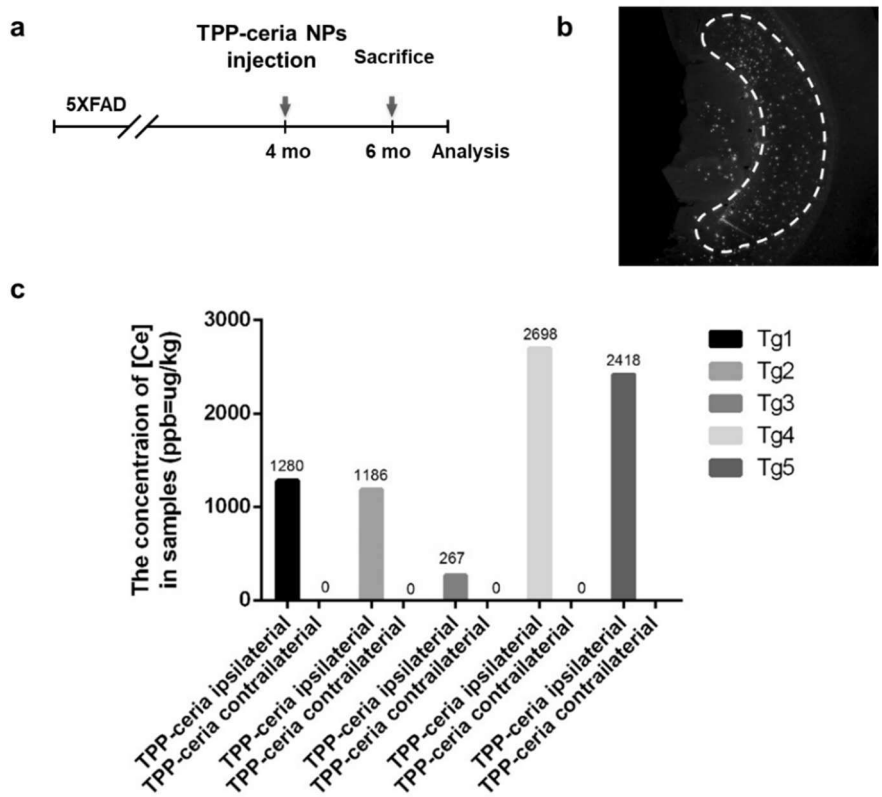

Figure 2.15. Stereotaxic injection of TPP-ceria nanoparticles into the subiculum of 5XFAD mice. a) Stereotaxic surgery was used to inject FITC-conjugated TPP-ceria NPs or PBS. Mice were sacrificed and the brains analysed by immunohistochemistry 2 months after injection. b) Confocal microscope image from brain sections of FITC-conjugated TPP-ceria NP-injected mice. c) The concentration of cerium ions in the ipsilateral and contralateral brain tissues were measured by ICS-MS.

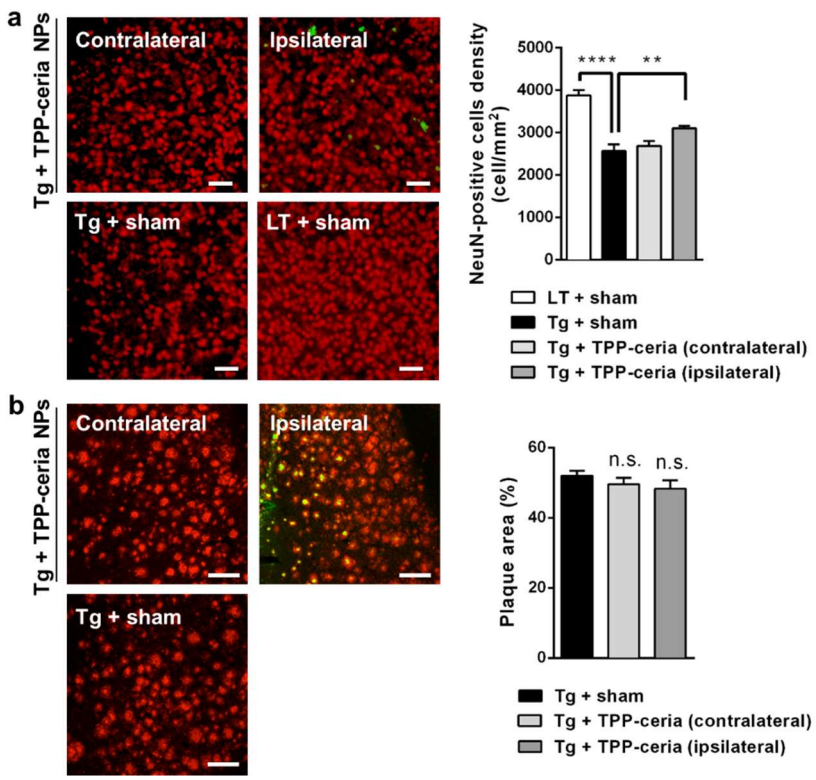

Figure 2.16. TPP-ceria NPs ameliorate neuronal loss, but not plaque deposition. (a) Confocal fluorescence images (left) of coronal brain sections stained with anti-NeuN antibody (red) and FITC-conjugated TPP-ceria NPs (green). Scale bar = 30 μm. Plot of neuronal cell density (right). Statistical analysis was performed using an ANOVA test. Error bars represent 95% confidence intervals (CI). ****$p < 0.0001$; **$p < 0.01$; LT + sham: littermate mice; Tg + sham: 5XFAD mice (n = 4 per group). (b) Confocal fluorescence images (left) of Aβ deposition in coronal brain sections stained with biotin-labeled 4G8 antibody (red) and FITC-conjugated TPP-ceria NPs (green) (n = 4 per group). Scale bar = 50 μm. Plot of plaque area (right). Statistical analysis was performed using an ANOVA test, with n.s. indicating no significance difference. Error bars represent 95% CIs.

2.3.6 Prevention of Abnormal Glial Activation.

To determine the mechanism how TPP-ceria NPs mitigate neuronal cell death in 5XFAD mice, I analyzed the effect of TPP-ceria NPs on inflammation related to astrocytic and microglial activation. Dual immunostaining with astrocyte (glial fibrillary acidic protein, GFAP) and microglia (ionized calcium binding adaptor molecule-1, Iba-1) markers shows enhanced GFAP and Iba-1 immunoreactivity in 6 month old 5XFAD mice, indicative of reactive gliosis. Interestingly, GFAP and Iba-1 immunoreactivity is significantly decreased in the ipsilateral side of TPP-ceria NP-injected 5XFAD mice subicula relative to those of sham injected mice (Figure 2.17a). These results suggest that mitochondrial ROS plays an important role in inflammation-induced neuronal loss. Moreover, I also confirm that Aβinduced mitochondrial ROS accumulation in U373 astrocytes can be ameliorated with TPP-ceria NP treatment (Figure 2.17b). Taken together, I believe that TPP-ceria NPs mitigate brain inflammation by reducing mitochondrial ROS levels.

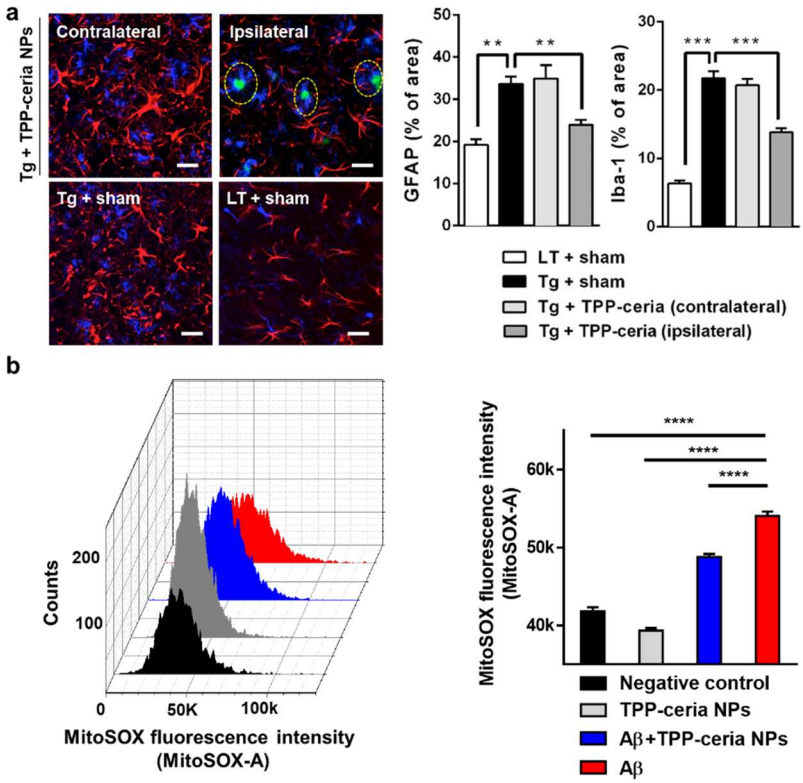

Figure 2.17. TPP-ceria NPs reduce reactive glial activation. (a) Confocal fluorescence images (left) of gliosis in tissue sections colabeled with GFAP (red) and Iba-1 (blue). Quantified levels of GFAP and Iba-1 in the images (n = 4 per group). Statistical analysis was performed using an ANOVA test. Error bars represent 95% CIs. **p < 0.01; ***p < 0.001; LT + sham: littermate mice; Tg + sham: 5XFAD mice. Scale bar = 30 μm. (b) Mitosox fluorescence intensity of mitochondrial ROS accumulation in U373 cells obtained by flow cytometry. U373 cells untreated (negative controls), exposed to 0.1 mM TPP-ceria NPs (TPP-ceria NPs), to 5 μMA β and 0.1 mM TPP-ceria NPs (Aβ + TPP-ceria NPs), and to 5 μMA β (Aβ) for 12 h were stained using 5 μM MitoSOX. Statistical analysis was performed using an ANOVA test. Error bars represent 95% CIs (****p < 0.0001).

2.3.7 Restoration of Mitochondrial Morphology from Damage by Oxidative Stress.

Alterations in mitochondria morphology are an early sign of ROS-induced mitochondrial dysfunction.[39,40] TEM analysis of mitochondria morphology in 5XFAD mice shows severe cristae disruptions and vacuolar shape in cells of subicula when I compare with wild-type counterparts. On the other hand, TPP-ceria NP-injected 5XFAD mice show normal cristae structures and healthy mitochondrial morphology. Furthermore, I find the nanoparticles inside the mitochondria in the TPP-ceria NP-injected mice, not in the vehicle-injected mice (Figure 2.18a). To validate these findings, in vivo ROS-scavenging properties of TPP-ceria NPs were examined by Western blot analysis. As expected, the level of the oxidative stress marker 4-hydroxynonenal (4-HNE), a major end product of lipid peroxidation, is significantly higher in the brains of 5XFAD mice than that of the wild-type counterparts. Consistent with the in vitro data, administration of TPP-ceria NPs decreases the level of 4-HNE, implying TPP-ceria NPs can effectively reduce oxidative stress signaling in mitochondria (Figure 2.18b,c).

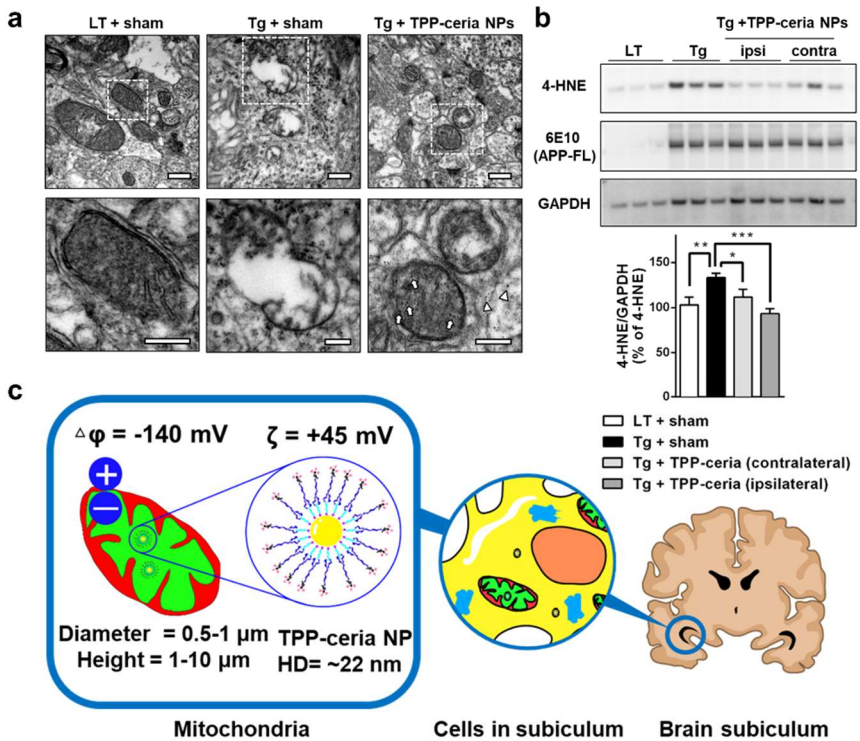

Figure 2.18. TPP-ceria NPs restore mitochondrial morphology and reduce oxidative stress. (a) TEM images showing representative mitochondrial morphologies of LT + sham, Tg + sham, and Tg + TPP-ceria NPs. Scale bar = 500 nm (n = 4 per group). Magnified images of the boxed areas are shown below. Arrows and arrowheads indicate TPP-ceria NPs in mitochondrial matrix and cytosol, respectively. Scale bar = 250 nm. (b) Western blot analysis for oxidative stress markers in 5XFAD mice treated with TPP-ceria NPs (n = 3 per group). Data were normalized with respect to the signal of GAPDH. Statistical analysis was performed using an ANOVA test. Error bars represent 95% CIs. *p < 0.05; **p < 0.01; ***p < 0.001; LT + sham: littermate mice; Tg + sham: 5XFAD mice. (c) TPP-ceria NPs localize to mitochondria of subicular cells due to their small hydrodynamic diameter (22 nm) and highly positive charge (+45 mV).

2.3.8 Discussion

While the molecular mechanisms of Aβ-induced mitochondrial dysfunction have not been fully elucidated, mitochondria are believed to be crucial contributors to AD pathogenesis. Numerous studies suggest that mitochondria promote cellular homeostasis by generating several redox enzymes, whereas abnormal ROS production decreases mitochondrial maintenance systems.[41] In neurodegeneration, the mitochondrial free-radical theory indicates that the progressive alteration of mitochondria that occurs with the aging process renders the increased production of ROS, which in turn causes further mitochondrial impairment and damage to the entire cells.[42] Based on these observations, abnormal ROS production and accumulation likely trigger cytosolic signaling pathways to induce intrinsic apoptosis. Current mitochondrial therapies for AD provide moderate symptomatic delay at various stages of the disease.[43,44] However, there still remain some unsolved questions. For instance, although mitochondrion-specific antioxidants based on small molecules can prevent ROS-mediated neuronal toxicity, they have limited ROS-scavenging activity due to their poor pharmacokinetic properties and irreversible activity, and therefore, they have to be administered continuously at high doses.[45,46] Ceria NPs

are highly stable in physiological conditions and exhibit recyclable antioxidant activity.[20-22,27] Consequently, they have shown potentials as a ROS-scavenging agent in various disease models, which also motivates their potential applications in neurodegenerative diseases.[21,23-26,47,48] Although recent studies have reported that ceria NPs can mitigate Aβ-induced mitochondrial dysfunctions in vitro,[49,50] the in vivo disease model study of ceria NPs on mitochondria has not been done yet. Neuronal loss is correlated to the severity of memory deficits in AD.[51,52] Our results demonstrate that TPP-ceria NPs act as an effective neuroprotectant in 5XFAD mice brains (Figure 2.16a). Despite these findings, TPP-ceria NPs do not seem to have any significant effect in reducing subicular Aβ deposition (Figure 2.16b), suggesting that the TPP-ceria NPs solely act as an antioxidant and do not eliminate Aβ plaques. Brain inflammation is a key inducer of neuronal loss in AD. Nonsteroidal anti-inflammatory drugs (NSAIDs) protect neurons without altering Aβ generation.[53,54] Similarly, TPP-ceria NP-treated 5XFAD mice show significantly lower expression of astrocyte and microglia inflammatory markers (Figure 2.17a). 4-HNE is an aldehyde byproduct of n6 fatty acid oxidation and is known to accumulate in various oxidative stress-related diseases, including AD.[55-57] I observe

that 4HNE production is also inhibited by the TPP-ceria NPs. Inflammasomes, such as NLRP3, AIM2, and NLRC3, are protein complexes that recognize inflammation-inducing stimuli, including ROS. It has recently been reported that Aβ activates the NLRP3 inflammasome to potentiate cerebral neuroinflammation.[58,59] As shown in Figure 2.17a, TPP-ceria NPs are predominantly colocalized to the microglial marker, Iba-1 (yellow circle). Furthermore, when I investigated nine slides of tissue sections, I did not observe any proportion of TPP-ceria NPs colocalized to the neuronal marker NeuN and the astrocytic marker GFAP (Figures 2.16a and 2.17a). Although exact mechanisms have yet to be elucidated, TPP-ceria NPs may ameliorate neuroinflammation by suppressing microglial activation. Microglia are master regulators of inflammasome activation and have an important role in the development of neurodegenerative disease, including AD.[59,60] It has also been reported that inhibition of microglial proliferation leads to prevention of synaptic degeneration.

2.4 Conclusion

In this study, I synthesized small and positively charged TPP-ceria NPs capable of localizing to mitochondria in various cell lines. TPP-ceria NPs are biocompatible and can scavenge mitochondrial ROS efficiently to reduce oxidative stress in vitro and in vivo. The TPP-ceria NPs mitigate the reactive gliosis and suppress neuronal death in a 5XFAD transgenic AD mouse model. Our results demonstrate a novel strategy for the development of mitochondrial therapeutics against neuroinflammation and have important implications for the treatment of AD and other neurodegenerative diseases.

**Most of the contents of this chapter were published in the article,

"Mitochondria-targeting ceria nanoparticles as antioxidants for Alzheimer's disease." (*ACS nano* **2016**, 10.2, 2860)

2.5 References

[1] J. L. Cummings, G. Cole, *Jama* **2002**, *287*, 2335.

[2] R. Jakob-Roetne, H. Jacobsen, *Angewandte Chemie International Edition* **2009**, *48*, 3030.

[3] H. W. Querfurth, F. M. LaFerla, *N Engl J Med* **2010**, *362*, 329.

[4] Y. Huang, L. Mucke, *Cell* **2012**, *148*, 1204.

[5] S. Tu, S.-i. Okamoto, S. A. Lipton, H. Xu, *Mol. Neurodegener* **2014**, *9*, 48.

[6] F. Kamenetz, T. Tomita, H. Hsieh, G. Seabrook, D. Borchelt, T. Iwatsubo, S. Sisodia, R. Malinow, *Neuron* **2003**, *37*, 925.

[7] M. G. Bartley, K. Marquardt, D. Kirchhof, H. M. Wilkins, D. Patterson, D. A. Linseman, *Journal of Alzheimer's Disease* **2012**, *28*, 855.

[8] B. Westermann, *Sci Signal* **2009**, *2*, pe29.

[9] A. Federico, E. Cardaioli, P. Da Pozzo, P. Formichi, G. N. Gallus, E. Radi, *Journal of the neurological sciences* **2012**, *322*, 254.

[10] J. Yun, T. Finkel, *Cell metabolism* **2014**, *19*, 757.

[11] M. T. Lin, M. F. Beal, *Nature* **2006**, *443*, 787.

[12] H. Du, L. Guo, F. Fang, D. Chen, A. A. Sosunov, G. M. McKhann, Y. Yan, C. Wang, H. Zhang, J. D. Molkentin, *Nature medicine* **2008**, *14*, 1097.

[13] J. W. Lustbader, M. Cirilli, C. Lin, H. W. Xu, K. Takuma, N. Wang, C. Caspersen, X. Chen, S. Pollak, M. Chaney, *Science* **2004**, *304*, 448.

[14] C. Schmidt, E. Lepsverdize, S. Chi, A. Das, S. Pizzo, A. Dityatev, M. Schachner, *Molecular psychiatry* **2008**, *13*, 953.

[15] L. M. Shaw, H. Vanderstichele, M. Knapik-Czajka, C. M. Clark, P. S. Aisen, R. C. Petersen, K. Blennow, H. Soares, A. Simon, P. Lewczuk, *Annals of neurology* **2009**, *65*, 403.

[16] H. Du, L. Guo, S. Yan, A. A. Sosunov, G. M. McKhann, S. S. Yan, *Proceedings of the National Academy of Sciences* **2010**, *107*, 18670.

[17] M. J. McManus, M. P. Murphy, J. L. Franklin, *The Journal of Neuroscience* **2011**, *31*, 15703.

[18] A. Eckert, K. L. Schulz, V. Rhein, J. Götz, *Molecular neurobiology* **2010**, *41*, 107.

[19] B. C. Dickinson, C. J. Chang, *Journal of the American Chemical Society* **2008**, *130*, 9638.

[20] A. Karakoti, S. Singh, J. M. Dowding, S. Seal, W. T. Self, *Chemical Society Reviews* **2010**, *39*, 4422.

[21] I. Celardo, J. Z. Pedersen, E. Traversa, L. Ghibelli, *Nanoscale* **2011**, *3*, 1411.

[22] A. S. Karakoti, S. Singh, A. Kumar, M. Malinska, S. V. Kuchibhatla, K. Wozniak, W. T. Self, S. Seal, *Journal of the American Chemical Society* **2009**, *131*, 14144.

[23] R. W. Tarnuzzer, J. Colon, S. Patil, S. Seal, *Nano letters* **2005**, *5*, 2573.

[24] J. Niu, A. Azfer, L. M. Rogers, X. Wang, P. E. Kolattukudy, *Cardiovascular research* **2007**, *73*, 549.

[25] J. Chen, S. Patil, S. Seal, J. F. McGinnis, *Nature Nanotechnology* **2006**, *1*, 142.

[26] S. Chigurupati, M. R. Mughal, E. Okun, S. Das, A. Kumar, M. McCaffery, S. Seal, M. P. Mattson, *Biomaterials* **2013**, *34*, 2194.

[27] C. K. Kim, T. Kim, I. Y. Choi, M. Soh, D. Kim, Y. J. Kim, H. Jang, H. S. Yang, J. Y. Kim, H. K. Park, S. P. Park, S. Park, T. Yu, B. W. Yoon, S. H. Lee, T. Hyeon, *Angewandte Chemie-International Edition* **2012**, *51*, 11039.

[28] M. P. Murphy, R. A. Smith, *Annu. Rev. Pharmacol. Toxicol.* **2007**, *47*, 629.

[29] S. Marrache, S. Dhar, *Proceedings of the National Academy of Sciences* **2012**, *109*, 16288.

[30] S. Biswas, N. S. Dodwadkar, P. P. Deshpande, V. P. Torchilin, *Journal of Controlled Release* **2012**, *159*, 393.

[31] T. Yu, J. Moon, J. Park, Y. I. Park, H. B. Na, B. H. Kim, I. C. Song, W. K. Moon, T. Hyeon, *Chemistry of Materials* **2009**, *21*, 2272.

[32] J. Park, K. An, Y. Hwang, J.-G. Park, H.-J. Noh, J.-Y. Kim, J.-H. Park, N.-M. Hwang, T. Hyeon, *Nature materials* **2004**, *3*, 891.

[33] S. Singh, A. Kumar, A. Karakoti, S. Seal, W. T. Self, *Molecular BioSystems* **2010**, *6*, 1813.

[34] K. Yang, Y.-Q. Ma, *Nature Nanotechnology* **2010**, *5*, 579.

[35] B. D. Chithrani, A. A. Ghazani, W. C. Chan, *Nano letters* **2006**, *6*, 662.

[36] H. Oakley, S. L. Cole, S. Logan, E. Maus, P. Shao, J. Craft, A. Guillozet-Bongaarts, M. Ohno, J. Disterhoft, L. Van Eldik, *The Journal of neuroscience* **2006**, *26*, 10129.

[37] J. Kreuter, *Advanced drug delivery reviews* **2014**, *71*, 2.

[38] S. I. Yoo, M. Yang, J. R. Brender, V. Subramanian, K. Sun, N. E. Joo, S. H. Jeong, A. Ramamoorthy, N. A. Kotov, *Angewandte Chemie International Edition* **2011**, *50*, 5110.

[39] A. B. Knott, G. Perkins, R. Schwarzenbacher, E. Bossy-Wetzel, *Nature Reviews Neuroscience* **2008**, *9*, 505.

[40] D.-F. Suen, K. L. Norris, R. J. Youle, *Genes & development* **2008**, *22*, 1577.

[41] J. Lee, J. H. Boo, H. Ryu, *Advanced drug delivery reviews* **2009**, *61*, 1316.

[42] C. López-Otín, M. A. Blasco, L. Partridge, M. Serrano, G. Kroemer, *Cell* **2013**, *153*, 1194.

[43] M. Manczak, P. Mao, M. J. Calkins, A. Cornea, A. P. Reddy, M. P. Murphy, H. H. Szeto, B. Park, P. H. Reddy, *Journal of Alzheimer's Disease* **2010**, *20*, 609.

[44] R. A. Smith, R. C. Hartley, H. M. Cocheme, M. P. Murphy, *Trends in pharmacological sciences* **2012**, *33*, 341.

[45] S. Nie, Y. Xing, G. J. Kim, J. W. Simons, *Annu. Rev. Biomed. Eng.* **2007**, *9*, 257.

[46] D. Peer, J. M. Karp, S. Hong, O. C. Farokhzad, R. Margalit, R. Langer, *Nature nanotechnology* **2007**, *2*, 751.

[47] K. L. Heckman, W. DeCoteau, A. Estevez, K. J. Reed, W. Costanzo, D. Sanford, J. C. Leiter, J. Clauss, K. Knapp, C. Gomez, *ACS nano* **2013**, *7*, 10582.

[48] B. Le Droumaguet, J. Nicolas, D. Brambilla, S. Mura, A. Maksimenko, L. De Kimpe, E. Salvati, C. Zona, C. Airoldi, M. Canovi, M. Gobbi, N. Magali, B. La Ferla, F. Nicotra, W. Scheper, O. Flores, M. Masserini, K. Andrieux, P. Couvreur, *ACS Nano* **2012**, *6*, 5866.

[49] J. Dowding, W. Song, K. Bossy, A. Karakoti, A. Kumar, A. Kim, B. Bossy, S. Seal, M. Ellisman, G. Perkins, *Cell Death & Differentiation* **2014**, *21*, 1622.

[50] A. Cimini, B. D'Angelo, S. Das, R. Gentile, E. Benedetti, V. Singh, A. M. Monaco, S. Santucci, S. Seal, *Acta biomaterialia* **2012**, *8*, 2056.

[51] W. Wei, L. N. Nguyen, H. W. Kessels, H. Hagiwara, S. Sisodia, R. Malinow, *Nature neuroscience* **2010**, *13*, 190.

[52] D. W. Wesson, R. A. Nixon, E. Levy, D. A. Wilson, *Molecular neurobiology* **2011**, *43*, 163.

[53] W. S. T. Griffin, *New England Journal of Medicine* **2013**, *368*, 770.

[54] N. H. Varvel, K. Bhaskar, M. Z. Kounnas, S. L. Wagner, Y. Yang, B. T. Lamb, K. Herrup, *The Journal of clinical investigation* **2009**, *119*, 3692.

[55] K. Uchida, *Progress in lipid research* **2003**, *42*, 318.

[56] S. Dalleau, M. Baradat, F. Guéraud, L. Huc, *Cell Death & Differentiation* **2013**, *20*, 1615.

[57] W. Xiang, S. Menges, J. C. Schlachetzki, H. Meixner, A.-C. Hoffmann, U. Schlötzer-Schrehardt, C.-M. Becker, J. Winkler, J. Klucken, *Molecular neurodegeneration* **2015**, *10*, 8.

[58] T. Strowig, J. Henao-Mejia, E. Elinav, R. Flavell, *Nature* **2012**, *481*, 278.

[59] M. T. Heneka, M. P. Kummer, A. Stutz, A. Delekate, S. Schwartz, A. Vieira-Saecker, A. Griep, D. Axt, A. Remus, T.-C. Tzeng, *Nature* **2013**, *493*, 674.

[60] D. Gomez-Nicola, V. H. Perry, *Systems Biology of Alzheimer's Disease* **2016**, 185.

Chapter 3. Ceria nanoparticle systems for selective scavenging of mitochondrial, intracellular, and extracellular reactive oxygen species in Parkinson's disease

3.1 Introduction

ROS, which are generated as natural products during the metabolism of oxygen, are essential for life owing to their functions, such as in cell signal transduction and immune response.[1,2] However, excessively produced ROS are deleterious in that they induce oxidative damages to biomolecules and cells.[3,5] As such, ROS are closely associated with the pathogenesis and progression of many diseases including cancers, cardiovascular diseases, neurodegenerative diseases, and sepsis.[6-11] Therefore, understanding the mechanism of ROS-induced oxidative stress in diseases is very important for developing potential therapy.

Based on their cellular localization, ROS can be classified as mitochondrial, intracellular, and extracellular ROS, all of which play distinctive roles in diseases. To eliminate these three types of ROS

selectively, here, I designed an assortment of ceria NPs (Scheme 3.1), by taking advantages of recent advances in NP synthesis and biomedical applications.[12-23] Ceria NPs effectively scavenge ROS using their catalase- and superoxide dismutase (SOD)-mimetic activities that originate from regenerative redox switching between Ce^{3+} and Ce^{4+} ions (Figure 3.1).[24-28] They readily penetrate cellular membrane and scavenge intracellular ROS in cytosol. Triphenylphosphonium (TPP)-conjugated ceria (TPP-ceria) NPs are capable of scavenging mitochondrial ROS after their delivery to mitochondria. Extracellular ROS are scavenged using ~300 nm-sized ceria NP clusters (cluster-ceria) that are not subject to cellular uptake.

These three kinds of ceria NPs were applied to treat PD. Although the mechanism of PD is quite complex, its pathological features, such as mitochondrial dysfunction, neuroinflammation, and neuronal death, manifest the influence of oxidative stress induced by mitochondrial, intracellular, and extracellular ROS.[32-35] Moreover, brain is much vulnerable to ROS because of its low antioxidant levels and abundance of lipids that are susceptible to oxidation.[36,37] All these aspects suggest PD as a useful candidate disease for studying the effects of selective ROS-scavenging. I compared the therapeutic efficacies of ceria, TPP-

ceria, and cluster-ceria NPs using an 1-methyl-4-phenyl-1,2,3,6-tetrahydropyridine (MPT P)-induced PD mouse model.[38]

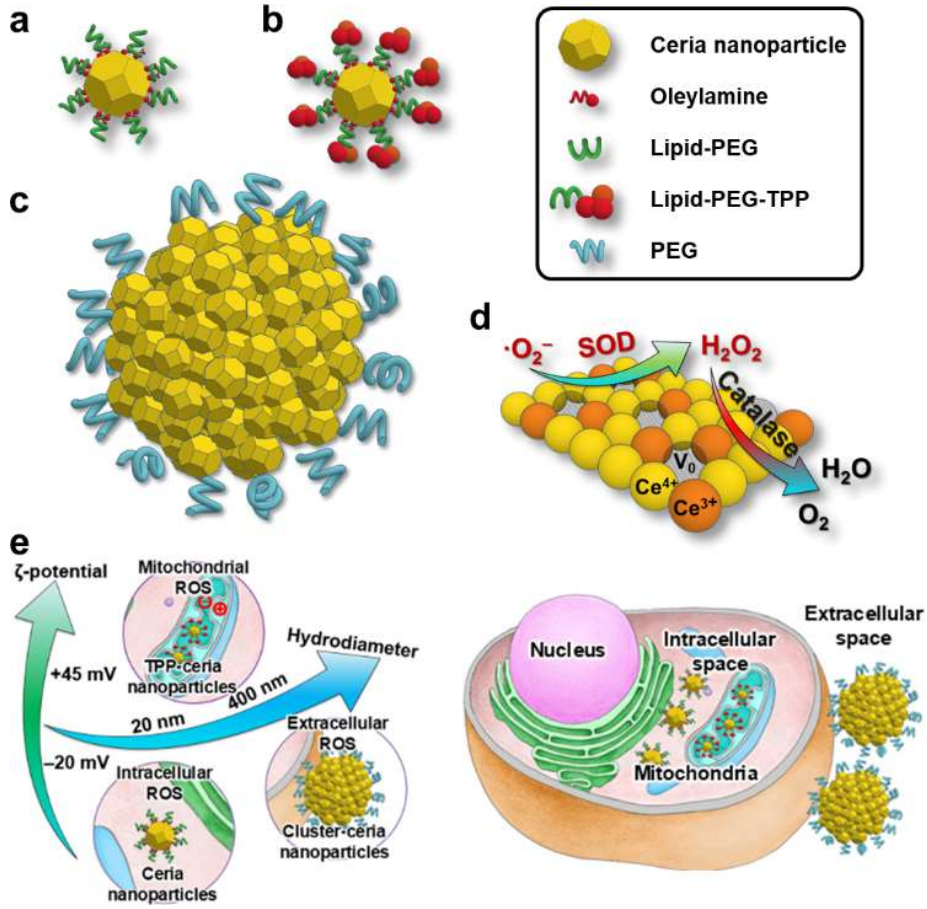

Scheme 3.1. Schematic illustrations: a) Ceria NP. b) TPP-ceria NP. c) Cluster-ceria NP. d) ROS scavenging reactions based on the SOD- and catalase-mimetic activities of ceria NPs. e) Cellular localization-dependent ROS scavenging activities of ceria, TPP-ceria, and cluster-ceria NPs.

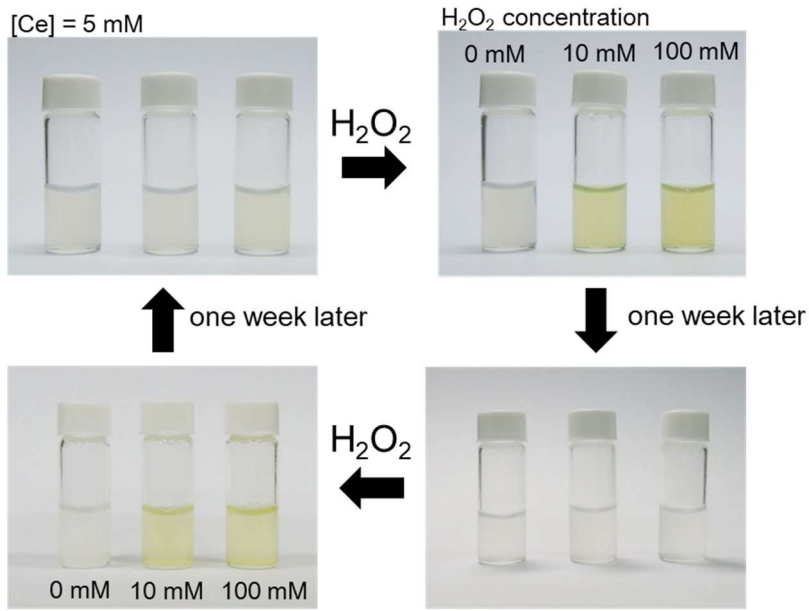

Figure 3.1. Photos showing the recyclable ROS scavenging activity of ceria nanoparticles. Among many types of ROS, H_2O_2 was used as an example for the demonstration. Higher concentrations than cellular levels were used to distinguish the color change with naked eye.

3.2 Experimental Section

3.2.1 Ceria nanoparticles.

3 nm ceria nanoparticles were synthesized as previously described. Briefly, a mixture solution of cerium(III) acetate (1 mmol), oleylamine (12 mmol) and xylene (15 mL) was stirred vigorously for 12 hours at room temperature, and then heated to 90 °C with a heating rate of 2 °C/min. Deionized (DI) water (1 mL) was injected rapidly into the solution to initiate a sol-gel reaction. The solution was kept at 90 °C for 3 hours, and then cooled to room temperature. Ceria nanoparticles were separated by centrifugation after adding acetone. The obtained ceria nanoparticles were dispersed in chloroform.

3.2.2 Water-dispersible ceria nanoparticles.

Ceria nanoparticles (8 mg) were mixed with 1,2-distearoyl-sn-glycero-3-phosphoethanolamine-N-[methoxy(polyethyleneglycol)-2000] (DSPE-PEG, Avanti Polar Lipids, Inc.) (25 mg) in chloroform (25 mL). After removal of the chloroform using a vacuum oven (80 °C), DI water (10 mL) was added, and the solution was sonicated. After filtration with a

syringe filter of 0.2 μm pore size, the ceria nanoparticles were separated by ultracentrifugation. The obtained ceria nanoparticles were purified by dialysis against water for 24 hours.

3.2.3 TPP-ceria nanoparticles.

TPP-ceria nanoparticles were obtained in a similar way to the preparation of water-dispersible ceria nanoparticles, except that TPP-conjugated DSPE-PEG was used. The TPP-conjugated DSPE-PEG was synthesized according to the previous report, and the conjugation was verified using a TOF 5800 mass spectrometry system installed at the National Center for Interuniversity Research Facilities at Seoul National University.

3.2.4 Cluster-ceria nanoparticles.

Cluster-ceria nanoparticles were prepared similarly to the reported method. Briefly, ceria nanoparticles (150 mg) in chloroform (4.5 g) were mixed with dodecyltrimethylammonium bromide (150 mg) in DI water (10 g). After removal of chloroform by evaporation, the solution was mixed with poly(acrylic acid) (0.9 g) in ethylene glycol (11 g). After

washing with DI water, cluster-ceria nanoparticles were separated by centrifugation. The obtained cluster-ceria nanoparticles were dispersed in DI water, and their surface was grafted with PEG-amine by a carbodiimide-mediated coupling reaction.

3.2.5 FITC-conjugated ceria, TPP-ceria, and cluster-ceria nanoparticles.

FITC-conjugated DSPE-PEG was prepared by reacting FITC (7.8 mg) with DSPE-PEG-amine (50 mg). To produce FITC-conjugated ceria or TPP-ceria nanoparticles, FITC-conjugated DSPE-PEG was used together with either DSPE-PEG or TPP-conjugated DSPE-PEG at the ratio of 1 to 50 during the water-transfer of ceria nanoparticles. To produce FITC-conjugated cluster-ceria nanoparticles, FITC-conjugated poly(allylamine) was used together with PEG-amine for the surface grafting of poly(acrylic acid)-coated cluster-ceria nanoparticles.

3.2.6 SOD- and Catalase-mimetic activity assays.

SOD-mimetic activity was assessed using a SOD assay kit (Sigma-

Aldrich). Ceria, TPP-ceria, or cluster-ceria nanoparticles were diluted in 200 μL of WST-1 (water-soluble tetrazolium salt; (2-(4-iodophenyl)-3-(4-nitrophenyl)-5-(2,4-disulfo-phenyl)-2H-tetrazolium, monosodium salt) solution with cerium concentrations of 0, 0.063, 0.125, 0.25, 0.5, and 1 mM, and added into microplate wells in triplicate. After adding xanthine oxidase (20 μL) into each well, the microplate was incubated at 37 °C for 20 minutes. Absorbance at 450 nm was measured for each well to evaluate the SOD-mimetic activity, where 50 U/mL SOD was defined as the amount of SOD that inhibits the reduction reaction of WST-1 by 50%. Catalase-mimetic activity was determined using the Amplex Red hydrogen peroxide/peroxidase assay kit (Molecular Probes Inc.). Ceria, TPP-ceria, or cluster-ceria nanoparticles were diluted to different cerium concentrations (0, 0.375, 0.75, and 1.5 mM) in a reaction buffer containing 100 μM Amplex Red reagent and 2 mM hydrogen peroxide. 50 μL of each solution was added into microplate wells in triplicate. The microplate was incubated at room temperature for 30 minutes, and absorbance at 490 nm was measured. 1 mU/mL HRP was used as a 100% control when estimating the catalase-mimetic activity.

3.2.7 Cell culture.

SH-SY5Y cells were cultured in a 1:1 mixture of minimum essential medium (MEM) and Ham's F12 medium. HeLa cells were cultured in Dulbecco's modified Eagle's medium (DMEM). Both cell culture media were supplemented with 10% heat-inactivated fetal bovine serum (FBS). Cells were maintained at 1×10^5 cells/mL at 37 °C in a humidified atmosphere of 5% CO_2.

3.2.8 Cell viability assays.

SH-SY5Y or HeLa cells were seeded (10,000 cells/well) in a 96-well plate and cultured for 24 hours. Ceria, TPP-ceria, or cluster-ceria nanoparticles were diluted in cell culture medium (0, 0.125, 0.25, 0.5, and 1 mM [Ce]), and added into the microplate wells in triplicate. The cells were incubated at 37 °C for 24 hours, and 20 μL of 3-[4,5-dimethylthialzol-2-yl]-2,5-diphenyltetrazolium diphenyltetrazolium bromide (MTT) (5 mg/mL) was added into each well. The cells were incubated at 37 °C for 4 hours, and then dimethyl sulfoxide (200 μL) was added into each well. Cell viability was determined by measuring absorbance at 595 nm.

3.2.9 Subcellular localization of nanoparticles.

SH-SY5Y or HeLa cells (1×10^5) were seeded in a confocal dish containing cell culture medium (2 mL), and the cells were incubated overnight. The medium was then replaced with fresh medium (2 mL) of 0.5 μM MitoTracker Orange CMTMRos (Invitrogen-Life Technologies) and 0.5 μM LysoTracker Blue DND-22 (Invitrogen-Life Technologies), and the cells were incubated at 37 °C for 30 minutes. Cells were washed three times with DPBS, and then cultured in cell medium containing FITC-conjugated ceria, TPP-ceria, or cluster-ceria nanoparticles at 37 °C for 4 hours. The medium containing FITC-conjugated ceria or TPP-ceria was then replaced with fresh medium (2 mL) after washing two times with PBS. Subcellular localization was investigated by confocal microscopy. Colocalization coefficients were calculated from the microscopic images.

3.2.10 Intracellular ROS-scavenging activity.

SH-SY5Y or HeLa cells were seeded (1×10^5 cells/well) in a 24-well

plate and cultured for 24 hours. Ceria, TPP-ceria, or cluster-ceria nanoparticles (0.1, 0.1, and 0.3 mM, respectively), were added to each well. The plate was incubated at 37 °C for 4 hours, at which point the cell culture medium of ceria or TPP-ceria nanoparticle-treated cells was replaced with new medium (1 mL). tBHP was added to a final concentration of 100 μM. The plate was incubated at 37 °C for 30 minutes. CellROX reagent was added to each well at a final concentration of 5 μM, and the plate was incubated for 30 minutes. The cells were washed three times with PBS. The cells were harvested by trypsinization and fixed in 3% formaldehyde for 10 minutes. The fixed cells were collected by centrifugation and resuspended in 0.5 mL PBS for flow cytometry analysis using a 473 nm laser and a 575 nm filter.

3.2.11 Mitochondrial ROS-scavenging activity.

The process was similar to that of intracellular ROS scavenging activity analysis, except that MitoSOX reagent was used instead of CellROX.

3.2.12 Extracellular ROS-scavenging activity.

The process was similar to that of intracellular ROS scavenging activity analysis, except that 1 mM hydrogen peroxide was used instead of tBHP.

3.2.13 Intracellular ROS induced by tBHP and H_2O_2

SH-SY5Y cells were seeded (1×10^5 cells/well) in a 24-well plate and cultured overnight. Cell culture medium was replaced with 2 ml DMEM (supplemented with 10% heat-inactivated FBS) containing tBHP or H_2O_2 (0, 0.125, 0.25, 0.5, and 1 mM). The plate was incubated at 37 °C for 30 minutes. CellROX reagent was added to each well at a final concentration of 5 μM, and the plate was incubated for 30 minutes. The cells were washed three times with PBS. The cells were harvested by trypsinization and fixed in 3% formaldehyde for 10 minutes. The fixed cells were collected by centrifugation and resuspended in 0.5 mL PBS for flow cytometry analysis using a 473 nm laser and a 575 nm filter.

3.2.14 Extracellular ROS induced by tBHP and H_2O_2

OxiSelect *in vitro* ROS/RNS assay kit (Cell Biolabs) was used to measure the ROS levels. SH-SY5Y cells were seeded (1×10^5 cells/well)

in a 6-well plate and cultured overnight. Cell culture medium was replaced with 2 ml DMEM (supplemented with 10% heat-inactivated FBS) containing tBHP or H_2O_2 (0, 0.125, 0.25, 0.5, and 1 mM). The plate was incubated at 37 °C for 30 minutes. 50 μL of supernatant was transferred into 96-well microplate wells in triplicate. 50 μL of diluted catalyst solution (Part No. 234703) was added to each well and incubated for 5 minutes. 100 μL of DCHF solution (Part No. 234704) was added to each well and incubated for 15 minutes. Fluorescence at 530 nm was measured using 480 nm excitation.

3.2.15 Animal model.

8-week-old male C57BL/6 mice (n = 6) received four subcutaneous injections of MPTP hydrochloride (20 mg/kg body weight) dissolved in saline at 2-hour intervals according to the published guideline[27]. Control mice received saline only. The mice were sacrificed 7 days after the last injection. Animal treatment and maintenance were approved by the institutional animal care and use committee of Seoul National University.

3.2.16 Stereotaxic injection.

Mice were anesthetized with isofluorane and placed in a stereotaxic frame. Striatum injections of saline (3 µl), FITC-conjugated ceria (0.1 mM, 3 µl), TPP-ceria (0.1 mM, 3 µl), or cluster-ceria nanoparticles (0.3 mM, 3 µl) was performed using the apparatus (0.62 mm AP, -2.0 mm ML, and -3.5 mm DV).

3.2.17 Immunoshistochemistry and immunohistofluorescence.

Mice were anesthetized with isofluorane, and perfused with 4% paraformaldehyde in PBS. Brains were subsequently fixed in 0.1 M phosphate buffer of 4% paraformaldehyde at 4 °C for 20 hours, and then incubated in 0.05 M PBS of 30% sucrose for 72 hours prior to sectioning into 30 µm slices using a cryostat. The tissue sections were incubated at 4 °C overnight with anti-TH antibody (1:1000, abcam ab112) or anti-IBA1 antibody (1:1000, ThermoFisher PA5-27436). HRP-conjugated anti-rabbit IgG antibody (1:500, abcam ab205718) and Alexa 647-conjugated anti-rabbit IgG antibody (1:500, ThermoFisher A-21245) were used as secondary antibodies for IHF and IHC, respectively.

3.2.18 Quantitation of 4-hydroxynonenal.

4-HNE was quantitated by HNE adduct competitive ELISA kit (Cell Biolabs). Proteins were extracted from 6 tissues of each treatment group using a homogenizer. Protein concentrations were normalized to glyceraldehyde 3-phosphate dehydrogenase.

3.3 Result and Discussion

3.3.1 Synthesis and characterization of ceria, TPP-ceria and ceria-cluster NPs

Ceria NPs with an average size of 3 nm were synthesized by a modified reverse micelle method (Figure 3.2a).[39,40] X-ray diffraction (XRD) analysis reveals the CeO_2 crystal structure of the ceria NPs (Figure 1d), and XPS data also shows the presence of Ce^{4+} ions on the NPs (Figure 3.2e). The ceria NPs were further encapsulated with polyethylene glycol (PEG) to provide water dispersibility and to prevent non-specific binding of biomolecules.[41] The hydrodynamic diameter and ζ-potential values of the water-dispersed ceria NPs are 11 nm and -23 mV, respectively (Figure 1f). The small hydrodynamic diameter of the ceria NPs enables their facile cellular uptake, as demonstrated in experiments performed using SH-SY5Y and HeLa cells (Figure 3.2g and 3.3). The internalized ceria NPs are found to localize in the cytoplasm. However, they do not penetrate into mitochondria possibly due to the electrostatic repulsion between negatively charged NP surface and inner mitochondrial membrane. In order to achieve the mitochondrial delivery, TPP-ceria

NPs were produced by encapsulating ceria NPs with TPP-conjugated PEG. TPP is a lipophilic cation with a known property of accumulating in mitochondria, and the prepared TPP-ceria NPs can internalize into mitochondria as expected (orange color in Figure 3.2h, 3.3 and 3.4). Although the TPP-ceria NPs do not show any discernible size or shape difference in the transmission electron microscopy (TEM) image compared with the ceria NPs (Figure 3.2b), their hydrodynamic diameter and ζ-potential values are changed to 22 nm and +45 mV, respectively (Figure 3.2f), reflecting the conjugation of TPP. Cluster-ceria NPs were obtained by assembling ~100,000 ceria NPs using an oil-in-water microemulsion technique (Figure 3.2c). Owing to their large size, endocytosis of the cluster-ceria NPs is blocked, and they remain in the extracellular space (Figure 3.2i). The hydrodynamic diameter and ζ-potential values of the cluster-ceria NPs are 400 nm and -20 mV, respectively (Figure 3.2f). All these kinds of ceria NPs do not show any noticeable aggregation in human plasma, and maintained their stability at least for one week (Figure 3.5).

MTT assays were performed to assess the viability of SH-SY5Y and HeLa cells after incubation with the ceria, TPP-ceria, or cluster-ceria NPs (Figure 3.2j; SI, Figure 3.6). Cluster-ceria NPs are the least toxic,

and high cell viability is maintained at concentrations as high as 1 mM [Ce]. Both ceria NPs and TPP-ceria NPs are non-toxic at concentrations less than 0.25 mM [Ce]. At higher concentrations, the TPP-ceria NPs are slightly more toxic than the ceria NPs. These results demonstrate that different localizations of the ceria, TPP-ceria, and cluster-ceria NPs affect their cytotoxicity.

ROS-scavenging activities of the ceria, TPP-ceria, and cluster-ceria NPs were evaluated using SOD and catalase activity assays (Figure 3.2k and 3.7). All types of the ceria NPs show dose-dependent activities in both assays, demonstrating their capabilities for scavenging superoxide ($^{\cdot}O_2^-$) and hydrogen peroxide (H_2O_2) using their SOD- and catalase-mimetic activities, respectively. The lower activity of the cluster-ceria NPs compared with the others can be ascribed to their lower surface-to-volume ratio.

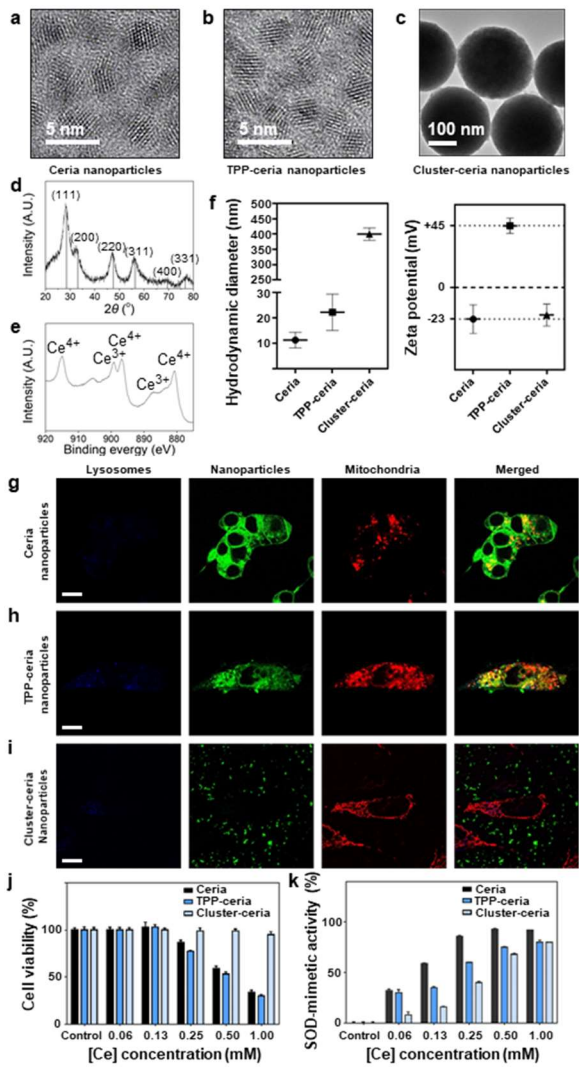

Figure 3.2. TEM images: a) Ceria NPs. b) TPP-ceria NPs. c) Cluster-ceria NPs. d) XRD pattern of ceria NPs (JCPDS No. 00-034-03494). e) XPS data of ceria NPs. f) Hydrodynamic diameters and zeta potential values. Confocal images of SH-SY5Y cells (lysosomes (blue), mitochondria (red), and FITC-conjugated NPs (green)): g) ceria NPs. h) TPP-ceria NPs. i) cluster-ceria NPs. Scale bars are 10 μm. j) MTT assay results performed for SH-SY5Y cells. k) SOD-mimetic activities.

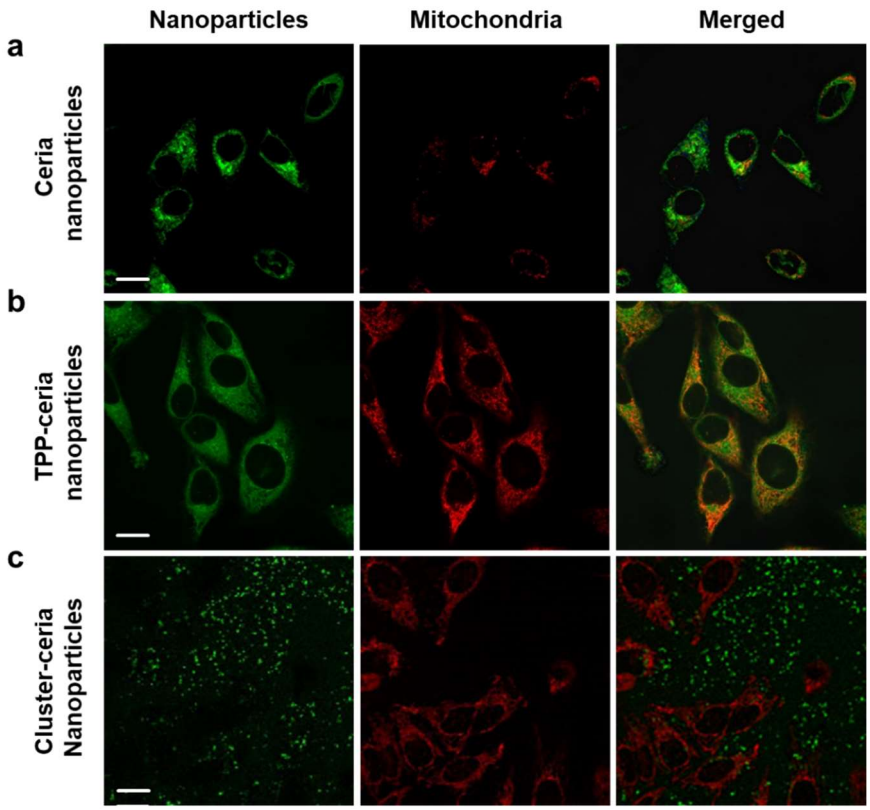

Figure 3.3. Confocal images of HeLa cells showing the cellular localizations of FITC-conjugated (a) ceria, (b) TPP-ceria, and (c) cluster-ceria nanoparticles. Scale bars are 10 μm.

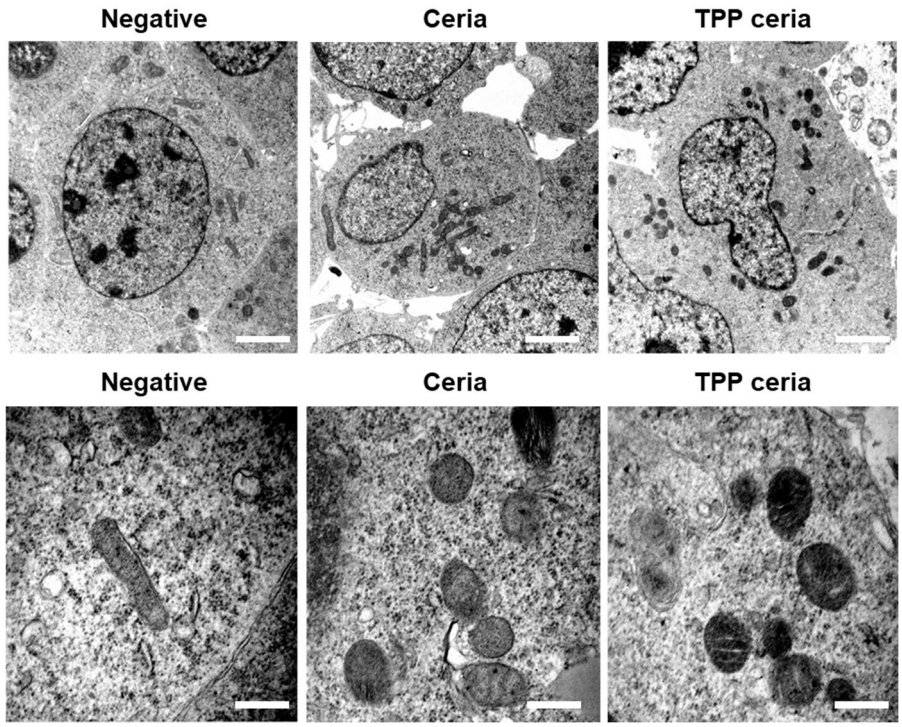

Figure 3.4. TEM images and magnified TEM images showing the subcellular distributions of ceria and TPP-ceria nanoparticles in SH-SY5Y cells. TPP-ceria nanoparticles can be seen in mitochondria. Scale bars are 500 (top row) and 2 (bottom row) μm.

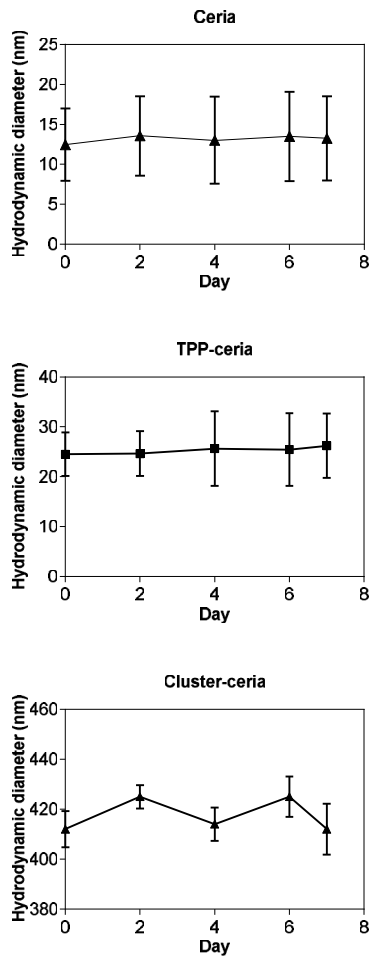

Figure 3.5. Hydrodynamic diameters of (a) ceria, (b) TPP-ceria, and (c) cluster ceria nanoparticles in human plasma monitored for a week.

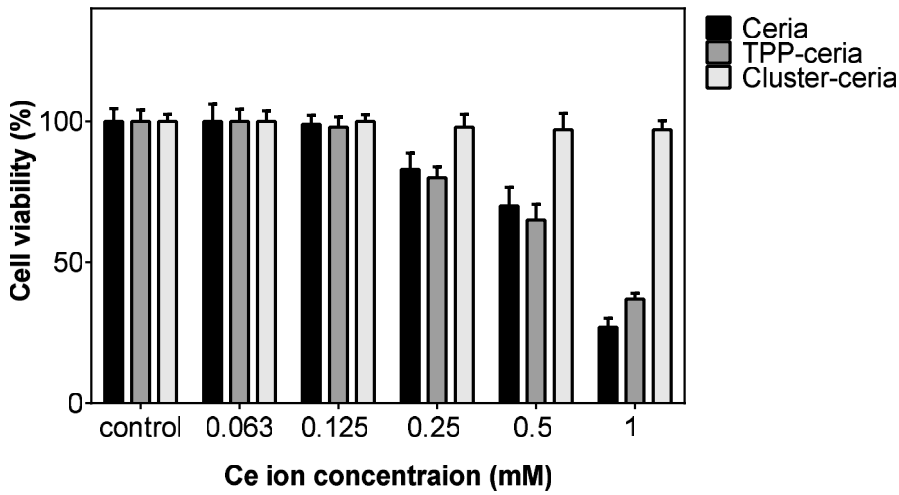

Figure 3.6. MTT assay results of ceria, TPP-ceria, and cluster-ceria nanoparticles performed for HeLa cells.

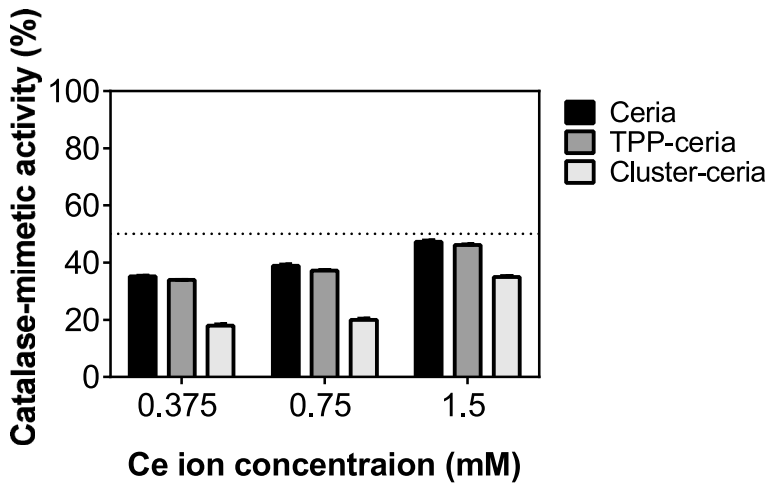

Figure 3.7. Catalase-mimetic activities of ceria, TPP-ceria, and cluster-ceria nanoparticles evaluated at different cerium ion concentrations.

3.3.2 Selective scavenging of mitochondrial, intracellular, and extracellular reactive oxygen species of ceria nanoparticle systems

ROS-scavenging effects of the ceria, TPP-ceria, and cluster-ceria NPs against intracellular, mitochondrial, and extracellular ROS were investigated using SH-SY5Y (Figure 3.8) and HeLa cells (Figure 3.9) *in vitro* by flow cytometry. To test the intracellular ROS-scavenging, the cells incubated in the absence or presence of each type of ceria NP (0.1, 0.1, and 0.3 mM for ceria, TPP-ceria, and cluster-ceria NPs, respectively) were treated with tert-butyl hydroperoxide (tBHP) (0.1 mM), and subsequently with CellROX reagent (5 μM), which is a cell-permeant fluorogenic probe that resides in cytoplasm and exhibits deep-red emission upon oxidation by ROS. tBHP induces higher degree of intracellular ROS than H_2O_2 of the same concentration (Figure 3.10), which is because the oxidative stress by tBHP is intensified through cell metabolism.[42] The subsequent oxidation of the CellROX inside the cells causes the fluorescence change (Figure 3.8a). Regarding the cells already loaded with the ceria NPs, CellROX does not show any fluorescence change because the oxidative stress generated by the cell-internalized tBHP is neutralized by the ceria NPs (Figure 3.8b). The TPP-ceria NPs

localized in mitochondria are not able to prevent the fluorescence change of the CellROX because they cannot eliminate the intracellular ROS (Figure 3.8c). The cluster-ceria NPs in the extracellular space cannot also prevent the fluorescence change of the CellROX taken by the cells because of their different localization (Figure 3.8d). Mitochondrial ROS-scavenging was demonstrated using tBHP (0.1 mM) and MitoSOX (5 μM), a mitochondrion-targeting fluorogenic probe with red emission that is sensitive to mitochondrial ROS (Figure 3.8e). Among the ceria NPs of different types, only the TPP-ceria NPs are able to minimize the fluorescence change of the MitoSOX (Figure 3.8g), while the other two types of the ceria NPs are not much effective (Figures 3.8f and h). Extracellular ROS-scavenging was investigated using CellROX (5 μM) and H_2O_2 (2 mM). Unlike tBHP, the oxidative stress of H_2O_2 takes place before its cellular uptake (Figure 3.10). The generated extracellular ROS can internalize into the cells and cause the fluorescence change of the CellROX in the cells (Figure 3.8i). The cluster-ceria NPs can scavenge those extracellular ROS, negating the oxidation-induced fluorescence change of the CellROX (Figure 3.8l). Considering that the cluster-ceria NPs cannot scavenge the intracellular ROS caused by tBHP, it is reasonable to assume that the cluster-ceria NPs are effective only to the

extracellular ROS. Besides, the ceria NPs loaded into the cells can also protect the CellROX from oxidation by the cell-internalized ROS, and thus can inhibit the fluorescence change (Figure 3.8j). The TPP-ceria NPs localized in mitochondria cannot interact with the cell-internalized ROS, allowing the fluorescence change of the CellROX (Figure 3.8k). All these data clearly show that the ceria, TPP-ceria, and cluster-ceria NPs eliminate intracellular, mitochondrial, and extracellular ROS, respectively (Figures 3.8m-o).

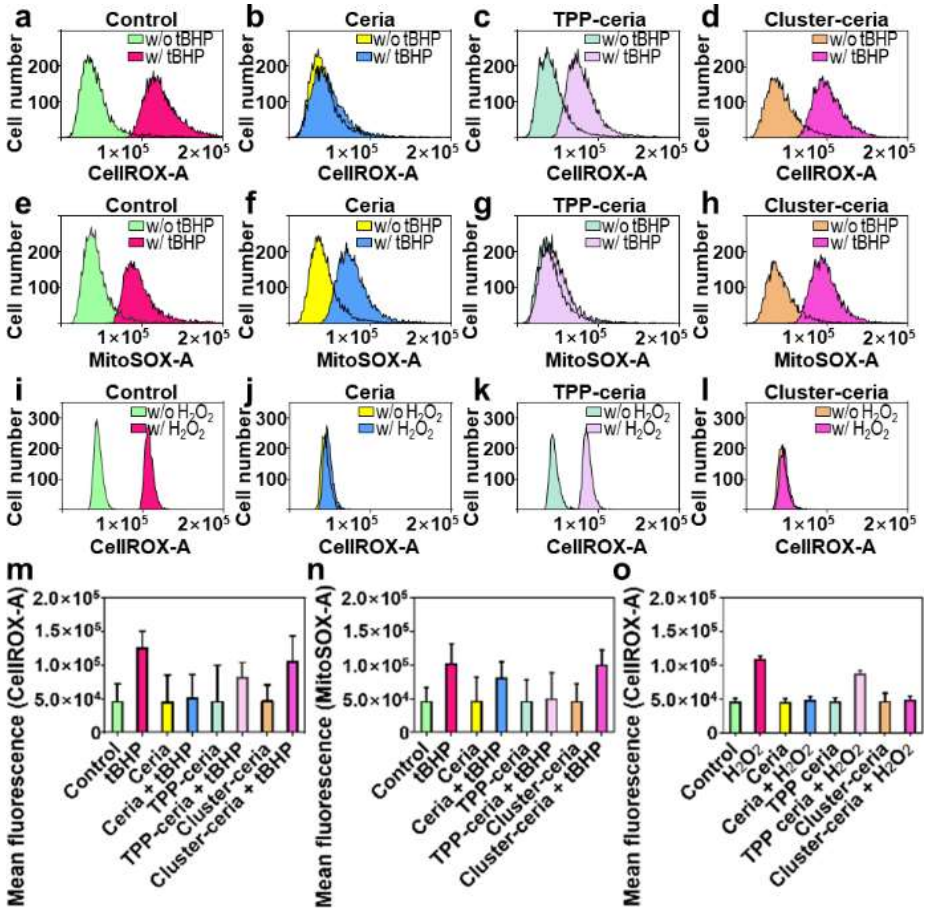

Figure 3.8. Fluorescence intensities of CellROX or MitoSOX measured for the tBHP- or H_2O_2-treated SH-SY5Y cells incubated without or with ceria, TPP-ceria, or cluster-ceria NPs: a) CellROX; tBHP; control. b) CellROX; tBHP; ceria. c) CellROX; tBHP; TPP-ceria. d) CellROX; tBHP; cluster-ceria. e) MitoSOX; tBHP; control. f) MitoSOX; tBHP; ceria. g) MitoSOX; tBHP; TPP-ceria. h) MitoSOX; tBHP; cluster-ceria. i) CellROX; H_2O_2, control. j) CellROX; H_2O_2; ceria. k) CellROX; H_2O_2; TPP-ceria. l) CellROX; H2O2; cluster-ceria. m) Summary of (a-d). n) Summary of (e-h). o) Summary of (i-l).

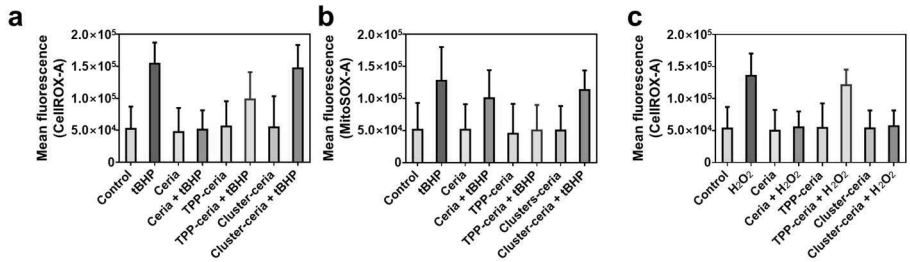

Figure 3.9. a) Summary of fluorescence intensities of CellROX measured for the tBHP-treated Hela cells incubated without or with various types of ceria nanoparticles. b) Summary of fluorescence intensities of MitoSOX measured for the tBHP-treated Hela cells incubated without or with various types of ceria nanoparticles. c) Summary of fluorescence intensities of CellROX measured for the H_2O_2-treated Hela cells incubated without or with various types of ceria nanoparticles.

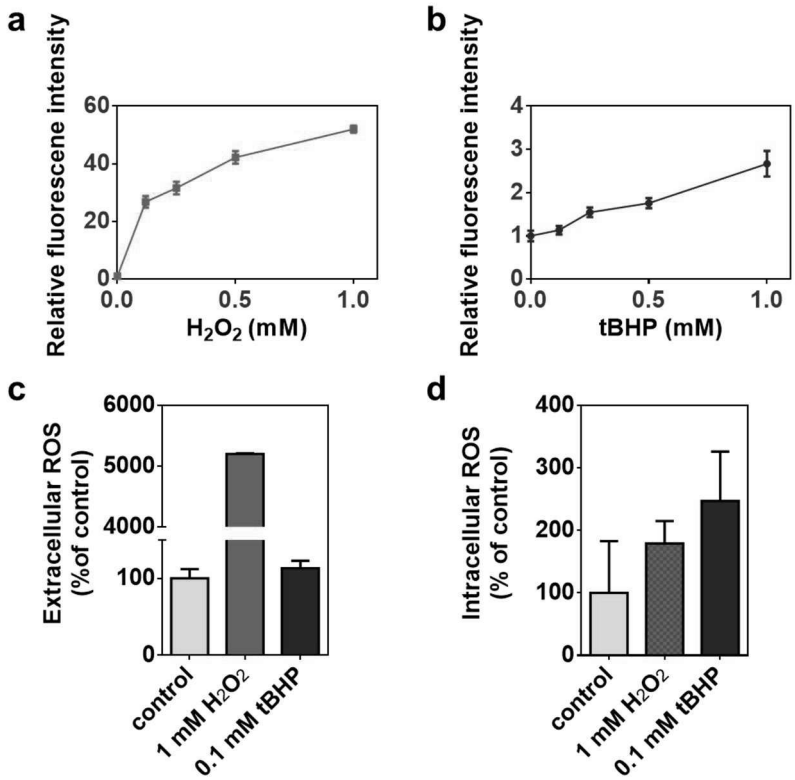

Figure 3.10. a) Relative fluorescence intensity of extracellular ROS induced by H_2O_2 at different concentrations. b) Relative fluorescence intensity of extracellular ROS induced by tBHP at different concentrations. c) Comparison of extracellular ROS levels induced by tBHP or H_2O_2 at the same concentrations used in the *in vitro* experiments. 4) Comparison of intracellular ROS levels induced by tBHP or H_2O_2 at the same concentrations used in the *in vitro* experiments.

3.3.3 *in vivo* therapeutic effects of the cellular localization-selective ROS-scavenging on the progression of PD

Next, I examined the *in vivo* therapeutic effects of the cellular localization-selective ROS-scavenging on the progression of PD. Each type of ceria NP (3 μl of 0.1, 0.1, and 0.3 mM solution for ceria, TPP-ceria, and cluster-ceria NPs, respectively) was administered to the right striata of C57BL/6 mice by stereotaxic injection 1 day after PD induction with MPTP. The mice were sacrificed at day 7 post-PD induction, and their coronal brain sections were analyzed. The presence of the ceria, TPP-ceria, or cluster-ceria NPs in the respective sections was verified by confocal microscopy using the fluorescence of the fluorescein isothiocyanate (FITC) conjugated onto the NPs (Figures 3.11a and b). The immunohistofluorescence (IHF) data (Figures 3.11a and c) reveal the increase of ionized calcium-binding adapter molecule 1 (IBA-1)-positive cells in the striata of the PD and sham groups compared with the wild-type mice. The upregulated expression of IBA-1 is indicative of the activation of microglia as a result of the increased neuroinflammation. [43] On the other hand, significantly reduced IBA-1 levels are observed for the ceria, TPP-ceria, and cluster-ceria NP-treated groups, which indicates that the ROS-scavenging effects of these kinds of NPs all

contribute to reduce the neuroinflammation. Changes in the striatal tyrosine hydroxylase (TH) levels upon treatment with different types of the ceria NPs were also monitored (Figures 3.11b and d). TH is an enzyme that converts L-tyrosine into levodopa, a precursor to produce neurotransmitter dopamine. Therefore, decreased level of TH, which is a hallmark of PD, reflects the degeneration of dopaminergic neurons in the nigrostriatal pathway that regulates the motor function. The PD and sham groups show obviously diminished TH levels. On the contrary, the ceria NP- and the TPP-ceria NP-treated groups exhibit significantly higher TH levels than the PD and sham groups. The cluster-ceria NP-treated group shows a similar TH level to those of the PD and sham groups, implying that scavenging extracellular ROS and reducing neuroinflammation are not effective to avoid the dopaminergic neuron degeneration. Lipid peroxidation, an indicator of oxidative damage,[44] was evaluated by measuring 4-hydroxynonenal (4-HNE) levels of each group (Figure 3.11e). The ceria NP- and the TPP-ceria NP-treated groups show significantly lower levels of 4-HNE compared with the PD group, whereas no significant difference is observed for the sham and cluster-ceria NP-treated groups. Our results suggest that the ceria NPs and the TPP-ceria NPs inhibit the degeneration of dopaminergic neurons by

alleviating the intracellular and mitochondrial oxidative stress, respectively. The overall distribution of TH was visualized by immunohistochemistry (IHC) of the brain sections. In the IHC data (Figure 3.12a), low levels of TH are apparent in the striatal regions of the PD, sham, and cluster-ceria NP-treated groups. In contrast, higher levels of TH are observed in the ceria or TPP-ceria NP-treated groups, which is on par with the previously discussed IHF data. These TH distributions are also visible in the confocal images (Figure 3.12b). Since the right striata of the mice were treated with a respective type of ceria NPs, only the ipsilateral regions exhibit the therapeutic effects of the ceria or TPP-ceria NPs—higher TH levels can only be seen in the left hemispheres of the brains. The fluorescence imaging also confirms the distribution of the ceria, TPP-ceria, or cluster-ceria NPs in the striatal regions Figure 3.12c).

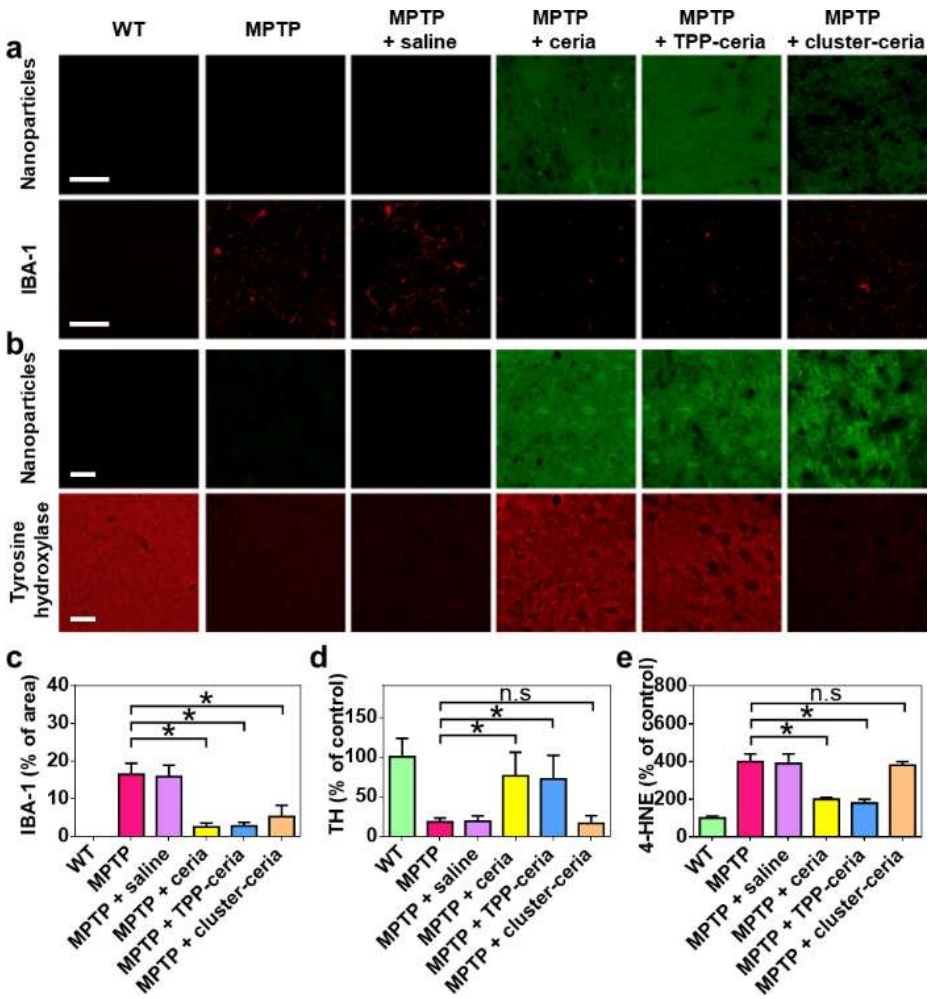

Figure 3.11 Confocal images of control and MPTP-induced PD mouse striata: a) FITC-conjugated NPs (top) and expression of IBA-1 (bottom). b) FITC-conjugated NPs (top) and expression of TH (bottom). Scale bars are 50 μm. Average expression levels of each treatment group: c) IBA-1. d) TH. e) 4-HNE. Error bars are ±1 standard deviation. One-way ANOVA was used for statistical analysis: *P < 0.0001, n.s. = non-significant.

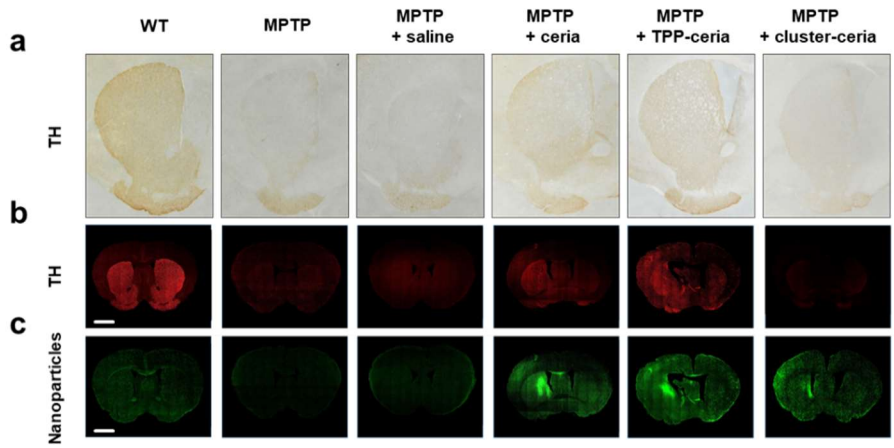

Figure 3.12. (a) Immunohistochemistry and (b) immunehistofluores - cence images showing the expression of TH in control and MPTP-induced PD mouse brains non-treated or treated with sham, ceria, TPP-ceria, and cluster-ceria nanoparticles. (c) Confocal images showing the distributions of ceria, TPP-ceria, or cluster-ceria nanoparticles in each group. Scale bars are 1 mm.

3.3.4 Discussion

The selective scavenging of ROS in different cellular localizations, as demonstrated in this study, can contribute to facilitate the future studies regarding the various roles of ROS. While the forms of biological ROS are mostly limited to hydrogen peroxide, superoxide, hydroxyl radical, and singlet oxygen, their physiological effects are much more diverse, which implies that the consequences of ROS-mediated chemical reactions should not be understood apart from their localization. In this respect, our ceria NP system will be able to provide an insight into the development of ROS-scavenging therapies for many diseases.

3.5 Conclusion

In summary, I developed a set of ceria NPs capable of scavenging mitochondrial, intracellular, and extracellular ROS selectively by tuning the NP localization in cells. These systems were applied to treat MPTP-induced PD mice not only to develop potential therapeutics but also to understand the roles of pathogenic ROS in PD. Scavenging intracellular ROS using the ceria NPs or mitochondrial ROS using the TPP-ceria NPs inhibits the neuroinflammation and lipid peroxidation, and also preserves the TH levels in the mouse striata. The observed neuroprotective effects seem to have resulted from the protection of axons of dopaminergic neurons against the oxidative stress. On the other hand, scavenging extracellular ROS using cluster-ceria NPs does not show any therapeutic effect in terms of lipid peroxidation and TH level, regardless of their efficacy to reduce neuroinflammation. These results suggest that lowering intracellular and/or mitochondrial oxidative stress is critical to treat PD, whereas extracellular ROS are not an effective treatment target to prevent neurodegeneration.

Most of the contents of this chapter will be published in the article, "Ceria nanoparticle systems for selective scavenging of mitochondrial, intracellular, and extracellular reactive oxygen species in Parkinson's disease." (*Angewandte Chemie*. **2018: doi:10.1002/anie.201805052)

3.5 References

[1] T. Finkel, N. J. Holbrook, *Nature* **2000**, *408*, 239.

[2] C. Nathan, A. Cunningham-Bussel, *Nature Reviews Immunology* **2013**, *13*, 349.

[3] R. S. Balaban, S. Nemoto, T. Finkel, *Cell* **2005**, *120*, 483.

[4] L. S. Lin, J. Song, L. Song, K. Ke, Y. Liu, Z. Zhou, Z. Shen, J. Li, Z. Yang, W. Tang, G. Niu, H. H. Yang, X. Chen, *Angewandte Chemie International Edition* **2018**, *57*, 4902.

[5] L. S. Lin, J. Song, L. Song, K. Ke, Y. Liu, Z. Zhou, Z. Shen, J. Li, Z. Yang, W. Tang, G. Niu, H. H. Yang, X. Chen, *Angewandte Chemie* **2018**, *130*, 4996.

[6] J. Cohen, *Nature* **2002**, *420*, 885.

[7] P. T. Schumacker, *Cancer Cell* **2006**, *10*, 175.

[8] M. T. Lin, M. F. Beal, *Nature* **2006**, *443*, 787.

[9] Z. Zhou, J. Song, L. Nie, X. Chen, *Chemical Society Reviews* **2016**, *45*, 6597.

[10] Z. Zhou, J. Song, R. Tian, Z. Yang, G. Yu, L. Lin, G. Zhang, W. Fan, F. Zhang, G. Niu, L. Nie, X. Chen, *Angewandte Chemie International Edition* **2017**, *56*, 6492.

[11] Z. Zhou, J. Song, R. Tian, Z. Yang, G. Yu, L. Lin, G. Zhang, W. Fan, F. Zhang, G. Niu, L. Nie, X. Chen, *Angewandte Chemie* **2017**, *129*, 6592.

[12] D. Kim, H. J. Kwon, K. Shin, J. Kim, R.-E. Yoo, S. H. Choi, M. Soh, T. Kang, S. I. Han, T. Hyeon, *ACS Nano* **2017**, *11*, 8448.

[13] J. Gao, H. Gu, B. Xu, *Accounts of Chemical Research* **2009**, *42*, 1097.

[14] D. Ni, J. Zhang, W. Bu, H. Xing, F. Han, Q. Xiao, Z. Yao, F. Chen, Q. He, J. Liu, S. Zhang, W. Fan, L. Zhou, W. Peng, J. Shi, *ACS Nano* **2014**, *8*, 1231.

[15] H. S. Choi, W. Liu, F. Liu, K. Nasr, P. Misra, M. G. Bawendi, J. V. Frangioni, *Nature Nanotechnology* **2009**, *5*, 42.

[16] C. Zhang, D. Ni, Y. Liu, H. Yao, W. Bu, J. Shi, *Nature Nanotechnology* **2017**, *12*, 378.

[17] X. Gao, Q. Yue, Z. Liu, M. Ke, X. Zhou, S. Li, J. Zhang, R. Zhang, L. Chen, Y. Mao, C. Li, *Advanced Materials* **2017**, *29*, 1603917.

[18] Y. Pan, X. Du, F. Zhao, B. Xu, *Chemical Society Reviews* **2012**, *41*, 2912.

[19] H. S. Choi, Y. Ashitate, J. H. Lee, S. H. Kim, A. Matsui, N. Insin, M. G. Bawendi, M. Semmler-Behnke, J. V. Frangioni, A. Tsuda, *Nature Biotechnology* **2010**, *28*, 1300.

[20] H. J. Kwon, K. Shin, M. Soh, H. Chang, J. Kim, J. Lee, G. Ko, B. H. Kim, D. Kim, T. Hyeon, *Advanced Materials* **2018**, 1704290.

[21] C. Carrillo-Carrion, M. Atabakhshi-Kashi, M. Carril, K. Khajeh, W. J. Parak, *Angewandte Chemie International Edition* **2018**, *57*, 5033.

[22] C. Carrillo-Carrion, M. Atabakhshi-Kashi, M. Carril, K. Khajeh, W. J. Parak, *Angewandte Chemie* **2018**, *130*, 5127.

[23] J. Hühn, C. Carrillo-Carrion, M. G. Soliman, C. Pfeiffer, D. Valdeperez, A. Masood, I. Chakraborty, L. Zhu, M. Gallego, Z. Yue, M. Carril, N. Feliu, A. Escudero, A. M. Alkilany, B. Pelaz, P. del Pino, W. J. Parak, *Chemistry of Materials* **2017**, *29*, 399.

[24] A. Karakoti, S. Singh, J. M. Dowding, S. Seal, W. T. Self, *Chemical Society Reviews* **2010**, *39*, 4422.

[25] M. Soh, D. W. Kang, H. G. Jeong, D. Kim, D. Y. Kim, W. Yang, C. Song, S. Baik, I. Y. Choi, S. K. Ki, H. J. Kwon, T. Kim, C. K.

Kim, S. H. Lee, T. Hyeon, *Angewandte Chemie International Edition* **2017**, *56*, 11399.

[26] M. Soh, D. W. Kang, H. G. Jeong, D. Kim, D. Y. Kim, W. Yang, C. Song, S. Baik, I. Y. Choi, S. K. Ki, H. J. Kwon, T. Kim, C. K. Kim, S. H. Lee, T. Hyeon, *Angewandte Chemie* **2017**, *129*, 11557.

[27] F. Zeng, Y. Wu, X. Li, X. Ge, Q. Guo, X. Lou, Z. Cao, B. Hu, N. J. Long, Y. Mao, C. Li, *Angewandte Chemie International Edition*.

[28] F. Zeng, Y. Wu, X. Li, X. Ge, Q. Guo, X. Lou, Z. Cao, B. Hu, N. J. Long, Y. Mao, C. Li, *Angewandte Chemie*.

[29] H. J. Kwon, M.-Y. Cha, D. Kim, D. K. Kim, M. Soh, K. Shin, T. Hyeon, I. Mook-Jung, *ACS nano* **2016**, *10*, 2860.

[30] H. Wang, Z. Feng, Y. Wang, R. Zhou, Z. Yang, B. Xu, *Journal of the American Chemical Society* **2016**, *138*, 16046.

[31] M. C. Rodriguez-Oroz, M. Jahanshahi, P. Krack, I. Litvan, R. Macias, E. Bezard, J. A. Obeso, *The Lancet Neurology* **2009**, *8*, 1128.

[32] D.-C. Wu, P. Teismann, K. Tieu, M. Vila, V. Jackson-Lewis, H. Ischiropoulos, S. Przedborski, *Proceedings of the National Academy of Sciences* **2003**, *100*, 6145.

[33] C. Henchcliffe, M. F. Beal, *Nature Clinical Practice Neurology* **2008**, *4*, 600.

[34] P. Jenner, *Annals of Neurology* **2003**, *53*, S26.

[35] E. Bossy-Wetzel, R. Schwarzenbacher, S. A. Lipton, *Nature Medicine* **2004**, *10*, S2.

[36] K. J. Barnham, C. L. Masters, A. I. Bush, *Nature Reviews Drug Discovery* **2004**, *3*, 205.

[37] T. Jiang, Q. Sun, S. Chen, *Progress in Neurobiology* **2016**, *147*, 1.

[38] V. Jackson-Lewis, S. Przedborski, *Nature Protocols* **2007**, *2*, 141.

[39] C. K. Kim, T. Kim, I. Y. Choi, M. Soh, D. Kim, Y. J. Kim, H. Jang, H. S. Yang, J. Y. Kim, H. K. Park, S. P. Park, S. Park, T. Yu, B. W. Yoon, S. H. Lee, T. Hyeon, *Angewandte Chemie International Edition* **2012**, *51*, 11039.

[40] C. K. Kim, T. Kim, I. Y. Choi, M. Soh, D. Kim, Y. J. Kim, H. Jang, H. S. Yang, J. Y. Kim, H. K. Park, S. P. Park, S. Park, T. Yu, B. W. Yoon, S. H. Lee, T. Hyeon, *Angewandte Chemie* **2012**, *124*, 11201.

[41] B. Pelaz, P. del Pino, P. Maffre, R. Hartmann, M. Gallego, S. Rivera-Fernández, J. M. de la Fuente, G. U. Nienhaus, W. J. Parak, *ACS Nano* **2015**, *9*, 6996.

[42] O. Kučera, R. Endlicher, T. Roušar, H. Lotková, T. Garnol, Z. Drahota, Z. Červinková, *Oxidative medicine and cellular longevity* **2014**, *2014*, 752506.

[43] X.-G. Luo, J.-Q. Ding, S.-D. Chen, *Molecular Neurodegeneration* **2010**, *5*, 12.

[44] A. Yoritaka, N. Hattori, K. Uchida, M. Tanaka, E. R. Stadtman, Y. Mizuno, *Proceedings of the National Academy of Sciences* **1996**, *93*, 2696.

Bibliography

1. Journal Publication

1) Hyek Jin Kwon, Moon-Yong Cha, Dokyoon Kim, Dong Kyu Kim, Min Soh, Kwangsoo Shin, Taeghwan Hyeon, and Inhee Mook-Jung. "Mitochondria-targeting ceria nanoparticles as antioxidants for Alzheimer's disease." *ACS nano* 10, no. 2 (2016): 2860-2870.

2) Hyek Jin Kwon, Kwangsoo Shin, Min Soh, Hogeun Chang, Jonghoon Kim, Jisoo Lee, Giho Ko, Byung Hyo Kim, Dokyoon Kim, and Taeghwan Hyeon. "Large-Scale Synthesis and Medical Applications of Uniform-Sized Metal Oxide Nanoparticles." *Advanced Materials* (2018): 1704290.

3) Hyek Jin Kwon, Dokyoon Kim, Kyungho Seo, Young Geon Kim, Sang Ihn Han, Taegyu Kang, Min Soh, Taeghwan Hyeon. "Ceria nanoparticle systems for selective scavenging of mitochondrial, intracellular, and extracellular reactive oxygen species in Parkinson's disease." *Angewandte Chemie*. (2018): doi:10.1002/anie.201805052

4) Dokyoon Kim, Hyek Jin Kwon, Kwangsoo Shin, Jaehyup Kim, Roh-Eul Yoo, Seung Hong Choi, Min Soh, Taegyu Kang, Sang Ihn Han, and Taeghwan Hyeon. "Multiplexible Wash-Free Immunoassay Using Colloidal Assemblies of Magnetic and Photoluminescent Nanoparticles." *ACS nano* 11, no. 8 (2017): 8448-8455.

5) Min Soh, Dong-Wan Kang, Han-Gil Jeong, Dokyoon Kim, Do Yeon Kim, Wookjin Yang, Changyeong Song, Hyek Jin Kwon, Taeghwan Hyeon*. et al. "Ceria-Zirconia Nanoparticles as Enhanced Multi-Antioxidant for Sepsis Treatment." *Angewandte Chemie*. 56, no. 38 (2017): 11399-11403

2. International Conferences

1) Hyek Jin Kwon, Moon-Yong Cha, Dokyoon Kim, Inhee Mook-Jung and Taeghwan Hyeon*, "Mitochondria-targeting ceria nanoparticles as a potential antioxidant drugs for therapy of Alzheimer's disease."

   2016 7th World congress of targeting mitochondria, Berlin, Germany

2) Hyek Jin Kwon, Moon-Yong Cha, Dokyoon Kim, Inhee Mook-Jung and Taeghwan Hyeon*, "Mitochondria-targeted ceria

nanoparticles as antioxidants drugs for Alzheimer's disease." 2016 MRS Boston USA

3) Hyek Jin Kwon, Moon-Yong Cha, Dokyoon Kim, Inhee Mook-Jung and Taeghwan Hyeon*, "Ceria nanoparticles targeted to mitochondrial reactive oxygen species as antioxidants drugs for Alzheimer's disease." 2016 ISNM Seoul Korea

4) Hyek Jin Kwon, Moon-Yong Cha, Dokyoon Kim, Inhee Mook-Jung and Taeghwan Hyeon*, "Mitochondria-targeting ceria nanoparticles conjugated triphenylphosphonium antioxidants for Alzheimer's disease." 2017 BDTS Seoul Korea

3. Awards

1) Best poster gold award 2016 ISNM Seoul Korea

2) Best poster award 2017 BDTS Seoul Korea

초 록

Ceria 나노 입자는 Ce^{3+} (환원) 및 Ce^{4+} (산화) 상태의 산화 환원 순환에 의해 활성 산소 종 (ROS) 및 활성 질소 종 (RNS)을 제거 할 수 있는 효과적인 항산화제이다. 또한, 5nm 미만의 크기를 갖는 세리아 나노 입자의 촉매 활성은 재활용되는 장점이 있다. 이러한 이유로 활성 산소가 유발하는 산화 스트레스에 의해 유발되는 다양한 질병에 대한 잠재적인 치료제 개발에 매우 적합하다. 이러한 배경으로 제 1 장에서는 의료용 세리아 나노 입자를 활용한 의학적 적용을 기술하였다.

제 2 장은 알츠하이머 질환에 대한 항산화제로서 미토콘드리아 표적 세리아 나노 입자를 합성하고 그 치료에 대한 효과를 기술하였다. 미토콘드리아 산화 스트레스는 알츠하이머병을 비롯한 신경 퇴행성 질환의 주요 병리학 적 요소이다. 미토콘드리아 기능 장애로 인해 활성산소가 비정상적으로 생성되면 신경 세포의 퇴행과 사멸을 야기한다. 세리아 나노 입자는 Ce^{3+}와 Ce^{4+} 산화 상태 사이를 왕복하면서 강하고 재활용 가능한 항산화제이다. 그래서, 세리아 나노 입자를

선택적으로 미토콘드리아로 표적화 하는 것은 신경 퇴행성 질환에 대한 유망한 치료법 일 수 있다. 그래서 세리아 나노입자 표면에 미토콘드리아 표적 물질인 Triphenylphosphonium (TPP) 를 결합시켜 TPP-세리아를 설계하고 합성하였다. 그리고 5XFAD 유전자 변형 알츠하이머 병 쥐 모델에 치료제로 사용해 보았다. 그 결과 TPP가 결합 된 세리아 나노 입자는 쥐의 뇌에서 미토콘드리아 손상을 완화, 산화적 스트레스 완화, 뇌염증 감소와 신경세포 사멸 감소의 치료 효과를 보였다. 이러한 결과들은 TPP가 접합 된 세리아 나노 입자가 알츠하이머 병에서 미토콘드리아 산화 스트레스의 잠재적인 치료 후보 물질이라는 것을 보여주었다.

제 3 장에서는 파킨슨 질병에서 미토콘드리아, 세포 내 및 세포 외 활성 산소를 선택적으로 제거하는 세리아 나노 입자 시스템에 대해 기술하였다. 활성 산소에 의해 유발 된 산화 스트레스는 많은 질병의 병인 및 진행에 중요한 요인 중 하나이다. 그러나, 세포내의 위치에 따라 활성산소를 제거하는 적절한 기술이 부족해 필수적인 그 병리학적 효과에 대한 이해와 연구가 가능하지 않다. 그래서 지금까지 개발된 기술을 활용하여 세리아 나노입자의 크기와 표면 성질을 다르게 해서

미토콘드리아, 세포 내 및 세포 외 활성 산소의 선택적 제거가 가능한 시스템을 개발 하였다. 이 시스템은 앞서 개발된 세포 내 표적 세리아, 미토콘드리아 표적 세리아 나노 입자와 세포 외 표적 세리아 나노 입자 덩어리로 구성되었다. 그리고 나는 이 시스템을 파킨슨 질병 모델 쥐 적용해 치료 연구를 해보았다. 그 결과 세포 내 또는 미토콘드리아 활성 산소를 제거하는 것이 파킨슨 모델 쥐의 선조체에서 타이로신 하이드록실레이즈를 보호하면서 신경세포의 퇴행성과 사멸을 방지하고, 별 아교 세포의 활성화 및 지질의 과산화에 의한 산화 스트레스를 억제한다는 것을 보여주었다. 이 결과는 파킨슨 질병의 진행에서 세포 내 및 미토콘드리아 활성산소의 필수 역할을 규명해주었다. 나는 세리아 나노입자 시스템이 다른 질병에서도 다양한 ROS의 기능을 밝히는데 유용한 도구로 사용될 것으로 기대한다.

주요어: 나노 입자, 세리아 나노 입자, 미토콘드리아, 알츠하이머 질병, 파킨슨 질병, 활성 산소, 항산화제, 미토콘드리아 활성 산소, 세포 밖 활성 산소, 세포내 활성 산소, 치매 치료제, 신경 퇴행성 질환,

학 번: 2013-30276